Lipid transfer by ORP3 is required for the regulation of PI4P and PI(4,5)P2 at the plasma membrane in mitosis

Anaïs Vertueux[1], Agathe Verraes[1], Christie Ouaddi[1], Emilie Pellier[2], Véronique Proux[1], Laurence Walch[3], Mélina Heuzé[1], Cathy L. Jackson[1], Jean-Marc Verbavatz[1#]

1 Université Paris-Cité, CNRS, Institut Jacques Monod, F-75013, Paris, France
2 CECS, I-Stem, INSERM U-861, Corbeil-Essonne, 91100, France
3 IEES Paris, Sorbonne Université, 75005 Paris, France
corresponding address: jean-marc.verbavatz@u-pariscite.fr

ABSTRACT

Lipid transfer proteins are an evolutionary-conserved families of proteins that transfer lipids at sites of contacts between the membrane of distinct organelles and contribute to the regulation of organelle-specific phospholipids, which set the organelle membrane identity and functions. In mitosis, PI(4,5)P2 accumulation at the plasma membrane is essential for the recruitment of the actomyosin cytoskeleton and the anchoring of the mitotic spindle at the plasma membrane. This is largely regulated by the function of kinases and phosphatases that interconvert phosphoinositide species. Here we demonstrate that during mitosis the ORP3 lipid transfer protein, which transfers PI4P from the plasma membrane to the endoplasmic reticulum (ER), indirectly regulates PI(4,5)P2 at the plasma membrane, in concert with the regulation by phosphoinositide kinases and phosphatases. Phosphorylation of a secondary ORP3 binding domain to the VAPA ER membrane protein strongly recruits ORP3 to the ER, where it is primed for PI4P transfer at ER-plasma membrane contact sites. Defects in ORP3 function during mitosis result in abnormal PI(4,5)P2 distribution and actin cytoskeleton, mitotic spindle geometry, abnormal cell division, and various cell division phenotypes, which lead to aneuploidy and eventually to cell death or genomic instability.

INTRODUCTION

In eukaryotes, the identity of cell membranes is defined by their specific lipid and protein composition (Jackson et al., 2016). Despite phosphoinositides (PIPs) are representing a minor fraction of membrane lipids (less than 1%, Cauvin et Echard, 2015), their distribution on the cytosolic leaflet of membrane compartments is exquisitely regulated. Different isoforms of phosphoinositides result from the interconversion by kinases and phosphatases of phosphate

groups at positions at position 3, 4 or 5 of the inositol ring of phosphoinositol (Mandal 2020). The resulting phosphoinositide diversity (7 species) and polarization at membranes is the foundation of cell membrane identity, which is essential for major cellular functions like membrane trafficking, cytoskeleton organization, dynamics and signaling (Posor et al., 2022). Phosphoinositides and their dynamics are crucial in mitosis to anchor and regulate the dynamics of the actomyosin and microtubule cytoskeleton at the plasma membrane through adaptor proteins (Cauvin et Echard, 2015). PI(4,5)P2 is the major phosphoinositide at the plasma membrane, where it binds a plethora of intracellular proteins (Mandal 2020), which among other functions are essential to recruit and shape the actin cytoskeleton (Senju et Lappalainen 2019), as well as microtubules (Gervais et al., 2008; Kotak et al., 2014). During mitosis, starting from prometaphase, thickening of the actin cortex leads to cell rounding, which is required to increase cell stiffness in order to support the forces required for cell elongation, chromosomes segregation and eventually cytokinesis and abscission. ERM proteins (Ezrin, Radixin, Moesin) bind PI(4,5)P2 at the plasma membrane and are also activated by PI(4,5)P2 ([Solinet et al., 2013). This is essential to anchor the cortical actin cytoskeleton, particularly in mitosis (Fehon et al., 2010). This is a highly regulated mechanism, as ERM proteins hyperactivation impairs cell elongation in anaphase due to increased the cortex stiffness (Roubinet et al., 2011), whereas ERM inhibition prevents cell rounding and impairs spindle assembly and chromosome segregation (Kunda et al., 2008). ERM activation in early mitosis is necessary for the localization of LGN-NuMA complex which defines the spindle orientation (Machicoane et al., 2014). In addition to ERMs, PI(4,5)P2 can directly recruit NuMA at the polar cortex (Kotak et al., 2014). During cytokinesis, PI(4,5)P2 accumulates at the ingression furrow, where it recruits components of the contractile ring, but PI(4,5)P2 hydrolysis also occurs in order to achieve a tightly regulated control of PI(4,5)P2 accumulation (Roubinet et al., 2011). Finally, prior to abscission,ERM proteins are inactivated and PI(4,5)P2 is hydrolyzed into PI4P at the site of abscission in order to depolymerize the actin cytoskeleton and allow for the recruitment of the ESCRT complex (Cauvin et al., 2015). Thus PI(4,5)P2 distribution at the cell cortex is a key determinant of proper mitosis from early steps into abscission and is tightly regulated in space and time.

PI(4,5)P2 is primarily produced from the phosphorylation of PI4P by PI4P 5-kinases (PI4P-5K), which are activated during mitosis and to a lesser extent from the hydrolysis of

PI(3,4,5)P3. At the plasma membrane, PI4P largely originates from vesicle trafficking in the secretory pathway. But PI4P can also result from the phosphorylation of PIPs by PI 4 kinases (PI-4K). Another source of membrane phosphoinositides comes from non-vesicular transfer of lipids by lipid transfer proteins. Lipid transfer proteins are recruited at sites of contact between the membranes of distinct organelles, where they can transfer lipids from one membrane to the other using a hydrophobic pocket (Weber-Boyvat et al., 2015; Reinisch et Prinz 2021). These membrane contacts often involve the endoplasmic reticulum (ER), which is the primary organelle of lipid synthesis (Yang et al., 2018).

ORPs (OSBP-related proteins) are one of the largest and best-studied families of lipid transfer proteins. The family has 12 members in humans (Delfosse et al., 2020). In mammals, most ORP proteins harbor 3 important domains: i) a FFAT motif (2 phenylalanines “FF” in an acidic tract), which specify ORP interaction with the MSP domain of VAP membrane proteins at the ER; ii) a “Plextrin Homology” (PH) domain, which binds membrane phosphoinositides and sometimes proteins on the target membrane; and iii) a hydrophobic lipid pocket (ORD domain) for the transfer of a lipid from one membrane to the other (Olkkonen, 2015; Delfosse et al., 2020). PI4P is one of the major substrates of ORP proteins since it is both a target of the PH domain of several ORPs (OSBP, ORP5, ORP8 ...) and a prominent substrate transported by the ORD domain (Jackson et al., 2016). PI4P transport by ORP proteins from the trans-Golgi, endosomes or the plasma membrane, where it is abundant, to the ER, where its concentrations are low is serving as the driving force for the counter-transport of another lipid (cholesterol, phosphatidylserine) against its gradient (Moser von Filseck et al., 2014; Mesmin et al., 2013; Mesmin et al., 2017) Phosphatidylserine transport by ORP5 and ORP8 from the ER to the plasma membrane was proposed to regulate PI4P availability, which is counter-transported from the plasma membrane to the ER (Sohn et al., 2018). Through the inter-conversion between PI4P and PI(4,5)P2 by kinases and phosphatases, this was proposed to regulate plasma membrane PI(4,5)P2 levels as well. However, this regulation of phosphoinositides at the plasma membrane is dependent on phosphatidylserine availability at the ER, to be counter-transported against PI4P.

Interestingly, one member of the ORP family, ORP3, localizes at ER-plasma membrane contacts and transfers PI4P from the plasma membrane to the ER against phosphatidylcholine (D’Souza et al., 2020), which, unlike phosphatidylserine is not a limiting lipid sepcies. Unlike most other plasma membrane ORPs, the PH domain of ORP3 was reported to bind primarily

PI(4,5)P2 and could therefore function as a PI(4,5)P2 sensor (D'Souza et al., 2020). We hypothesized that through efficient PI4P transfer from the plasma membrane to the ER and interconversion with PI(4,5)P2, ORP3 could regulate PI(4,5)P2 at the plasma membrane. ORP3 is involved in complex cellular processes dependent on PI(4,5)P2, such as cell adhesion, migration (Lehto et al., 2005; D'Souza et al., 2020), and actin dynamics (Lehto et al., 2008). Recent studies have linked ORP3 misregulation with aneuploidy and cancer development (Njeru et al., 2020; Wang et al., 2023; Xu et al., 2020). Hence, we investigated the potential role of PI(4,5)P2 regulation at the plasma membrane in mitosis. Our results in HeLa cells demonstrate that ORP3 is required for PI(4,5)P2 homeostasis in mitosis and for PI4P extraction for the cytoplasmic bridge in abscission. ORP3 is strongly recruited to the ER and to ER-plasma membrane contacts throughout mitosis. ORP3 depletion or inactivation results in abnormal PI(4,5)P2, PI4P, and actin cytoskeleton distribution at the plasma membrane in mitosis, leading to severe division defects.

RESULTS

ORP3 inactivation impairs chromosome segregation in mitosis and cell division.

In order to study the function of ORP3 in mitosis, we have established ORP3-KO HeLa cell lines, using a single nickase CRISPR-Cas9 strategy. Scrambled guide-RNAs were used to generate control CRISPR-Mock HeLa cell lines. Several independent clones were selected and tested by immunofluorescence and Western blotting (Fig. 1A, B). We confirmed that ORP3 was still present in CRISPR-Mock cells, where it is mostly cytosolic, just like in wild-type (WT) cells, but absent in the ORP3-KO cell lines. As recently reported (Wang et al., 2023), we observed that ORP3 depletion resulted in a significant increase of multinucleated cells, compared to WT or Mock cell lines in 3 different ORP3-KO clones tested (Fig. 1 C, D). Based on this consistent phenotype between various clones, only clone ORP3-KO1 was used in most of the following experiments. To investigate the course of events responsible for the accumulation of multinucleated cells, we examined the segregation of chromosomes in mitosis by live cell imaging (Fig. 1E). In WT cells, chromosome segregation from prophase to the end of anaphase took an average 1 hour. ORP3-KO cells exhibited a variety of phenotypes. Some ORP3-KO cells behaved just like control cells (Fig. 1E WT, vs KO line 1a), while other presented various defects in chromosome segregation. These defects ranged

from lagging chromosomes (Fig. 1E KO line b), chromosomes stuck in the midbody (Fig. 1E, line c), or the absence of segregation and DNA segregated in only one of the two daughter cells (Fig. 1E, line 4d). Additionally, a phenotype of abscission failure, where the two daughter cells re-merged at the end of cytoknesis, was sometimes observed in ORP3 KO cells (Movie 1). Altogether one or more division defects were detected in more than 50% of the cells in ORP3-KO cells and it was increased ~ 6-fold compared to WT or mock cells (Fig. 1F). Some of these defects resulted in aneuploidy and eventually to the accumulation of multinucleated cells, as seen in Fig. 1C. These defects are likely to activate the spindle assembly checkpoint and to result in mitotic delays. In WT and Mock cells, the duration of mitosis, between nuclear envelope breakdown and the beginning of DNA decondensation presented a unimodal distribution between 45 and 75 minutes (Fig. 1G). ORP3 KO cells were distributed into 3 distinct populations. Less than half (48%) behaved like WT cells, the majority of cells (52%) exhibited a strong increase in the duration of cell division between 75 and 115 min (class II 23%), or up to 135 min (class III 29%), almost doubling the duration of mitosis. To determine if the division phenotypes observed in ORP3-KO cells could arise as primary consequences of ORP3 depletion, as opposed to indirectand/or cumulative effects in stable cell lines, transient ORP3 depletion by siRNA treatment of WT HeLa cells was performed. Two distinct siRNAs resulted in a decrease in ORP3 protein signal in immunofluorescence and Western blots (Fig. 1H, I). Like ORP3-KO cells, ORP3 siRNA-treated cells exhibited various division defects, with a significant increase in frequency compared to scrambled control siRNA (Fig. 1J). Like in ORP3-KO cells, ~ 50% of cells showed at least one defect. In summary, our results suggest that ORP3 depletion results in chromosome segregation defects and delayed mitosis in more than 50% cell divisions, resulting in ~15% multinucleated cells at steady state. We hypothesize that these cells are eventually eliminated, resulting in a constant ploidy in the ORP3 KO cell population with no significant accumulation of ploidy defects in established cell lines. Accordingly, ORP3 KO cell proliferation in culture was significantly lower [not shown].

Every major ORP3 domain contributes to its function in mitosis

ORP3 functions at membrane contact sites between the ER - where it binds VAP proteins through its FFAT motif - and the plasma membrane - where it binds PI(4,5)P2 through its “Plextrin Homology” (PH) domain (Fig. 2A). The ORD domain of ORP3 can transport PI4P

from the plasma membrane to the ER and is believed to counter-transport phosphatidylcholine (D'Souza et al., 2020; Gulyás et al., 2020). A specificity of ORP3 is the existence of an additional non-canonical FFAT-like motif, which requires phosphorylation to become active (see Fig. 4D) (Weber-Boyvat et al., 2015). This FFAT-like domain was hypothesized to be a regulator, but its contribution to ORP3 function remains unknown. To assess the importance of ORP3 domains to cell division, we performed rescue experiments in ORP3-KO cells. Stable HeLa ORP3-KO cells were stably transfected with either wild-type GFP-ORP3, or the different GFP-ORP3 mutants shown in Fig. 2B. In interphase, GFP-ORP3 and "dead" mutants in the FFAT motif (E^{450}FFDAQE^{456} -> E^{450}VVAQUE^{456}) or in the FFAT-like motif (H^{161}FFSGST^{167} -> H^{161}VVAGST^{167}) were mostly cytosolic, just like endogenous ORP3 (Fig. 2C). The expression of a protein of expected size at expression levels comparable to WT cells was confirmed by Western blotting using anti-ORP3 antibodies (Fig. 2D). The frequency of multinucleated cells, which is the ultimate phenotype of ORP3-KO cells, was used as a readout for the rescue of ORP3 function (Fig. 2E). As expected, Hela WT cells and Mock-KO HeLa have a low frequency of multinucleated cells. GFP-WT-ORP3 fully rescued the multinucleated phenotype. This confirms that the mitotic ORP3-KO phenotype does not result from the accumulation of aneuploidy defects in ORP3-KO cell lines. In contrast, stable cell lines expressing mutants in any of PH, FFAT-like, FFAT or ORD domains of ORP3 all exhibited elevated frequencies of multinucleated cells, with no or limited rescue of the ORP3-KO phenotype. This is strongly suggesting that the lipid transfer function of ORP3 and localization at ER-plasma membrane contacts are all necessary necessary for proper cell division. In addition, our results also demonstrate that the often-overlooked FFAT-like motif is also essential to ORP3 function in mitosis. This is consistent with the idea that ORP3 can be "activated" through this domain, as previously proposed in response to PLC signaling (Gulyás et al., 2020). Deletion of the DLSK sequence of the ORD domain (Δ538-542), located in the lid of the hydrophobic pocket of ORP3 (Tong et al., 2021), further demonstrates that the transfer of lipid is also essential for proper division, beyond the mere presence of the ORD domain.

ORP3 is dramatically recruited to the ER by VAPA in mitosis

The ORP3 localization domains are required for cell division, yet, as shown in Fig. 2C and Fig. 3A (top inset), ORP3 is mostly cytosolic in interphase and only weakly ER- or plasma membrane-associated. Therefore, we investigated the localization of ORP3 during mitosis in ORP3-KO HeLa cells stably expressing GFP-ORP3 by live-cell imaging in spinning disk confocal microscopy (Fig. 3A). From prometaphase, when the ER starts tubulating, up until telophase (Puhka et al., 2007), ORP3 exhibited a dramatic change in subcellular localization, which was reminiscent of ER in mitosis, suggesting that ORP3 strongly localizes to the ER. ORP3 was also heavily present at the cell cortex and poles (Fig. 3A), suggesting that it could function at ER-plasma membrane contacts all along mitosis. On the other hand, ORP3 did not appear to be strongly localized to the ingression furrow in late anaphase-telophase-cytokinesis (Fig. 3A), despite higher PI(4,5)P2 levels (the target of ORP3 PH domain) reported at this location (Roubinet et al., 2011). In late cytokinesis, prior to abscission, ORP3 staining was restored to a diffuse localization in the cytosol, in addition to a strong enrichment at the midbody (Fig. 3A, bottom inset). The presence of ER-plasma membrane contacts in mitosis has been debated (Yu et Machaca 2025). We have confirmed their existence using the ER-PM contacts probe GFP-mapper (Fig. 3B), which showed a dense punctate staining at the plasma membrane of this ER-associated protein all along mitosis. ER-plasma membrane contacts were also observed during mitosis by electron microscopy, even in ORP3-KO cells (Fig. 3E). To confirm the recruitment of ORP3 at the ER in mitosis, we studied co-localization of WT GFP-ORP3 and mCherry-VAPA in live-cell imaging in ORP3-KO HeLa cells (Fig. 3C, top - metaphase shown). Both proteins strongly co-localized in the subcellular compartment. In addition, ORP3 (left) exhibited a strong punctate staining at the cell cortex, reminiscent of the GFP-mapper pattern. These results suggest that ORP3 is recruited at the ER throughout mitosis and is probably also located at ER-plasma membrane contacts. We next investigated the molecular basis for ORP3 localization at the ER during mitosis. First, we examined whether the FFAT motifs of ORP3 (FFAT and FFAT-like) (Fig. 3D pink and grey respectively) were involved in ORP3 localization during mitosis. As shown in Figure 3C, mutation in either one of the two FFAT motifs ($FFAT^m$ and $FFAT\text{-}like^m$) was not sufficient to delocalize ORP3 from VAPA at the ER in mitosis (Fig. 3C, lines 2 and 3). However, in double $FFAT^m$-$FFAT\text{-}like^m$ mutants, ORP3 became totally cytosolic (Fig. 3C, bottom line). These results demonstrate that both the canonical FFAT domain (as expected) and non-canonical FFAT-like domain independently contribute to ER localization of ORP3 during mitosis. We then

examined whether the ER localization of ORP3 was dependent on its ER anchoring partners: the VAP proteins. In HeLa cells, VAPA is the most abundant VAP (Di Mattia et al., 2018). A VAPA-KO HeLa cell line was created using a double nickase CRISPR-Cas9 strategy. Several clones were produced (two shown). The VAPA signal was abolished both in immunofluorescence (Fig. 3F) and in Western blotting (Fig. 3G). Importantly, VAPA deletion did not change the expression of the less abundant VAPB protein (Fig. 3G). In VAPA-KO HeLa cells, WT-ORP3 was no longer recruited to the ER in mitosis (Fig. 3H). Transfection of VAPA-KO cells with a CRISPR resistant VAPA rescued the ORP3 localization, but not transfection with a “dead” VAPA, mutated in its domain of interaction with FFAT motifs (MSP domain) (Fig. 3H, VAPA KD/MD). We conclude that during mitosis, ORP3 is strongly recruited by VAPA to the ER through both canonical (FFAT) and non-canonical (FFAT-like) motifs. Part of the ER-associated ORP3 is located at the cell cortex, where ER-plasma membrane contact sites may allow its function. Accordingly, ORP3 exhibits a punctate staining at the cortex in metaphase, reminiscent of the localization of GFP-mapper a probe for ER-plasma membrane contact sites.

The recruitment of ORP3 by VAPA to the ER is enhanced by phosphorylation of the ORP3 FFAT-like domain.

The interaction between VAPA and ORP3 in interphase and mitosis was further investigated by the study of ORP3 co-immunoprecipitation with VAPA, using a double Thymidine Nocodazole block to synchronize cells in G2/M (Fig. 4A). The abundance of VAPA in the input was not changed by the block, nor was the total abundance of ORP3 (Fig. 4A, input). However, there was a shift in the migration of ORP3 bands in synchronized cells, suggesting a post-translational modification of ORP3 at the onset of mitosis. In both non-synchronized and synchronized cells, VAPA successfully immunoprecipitated ORP3 (Fig 4A, IP). However, in addition to the migration-shift, the amount of immunoprecipitated ORP3 was much higher in synchronized cells, suggesting a strong increase in the interaction between VAPA and ORP3 in prometaphase, which is consistent with the ORP3 recruitment at the ER observed in live-cell imaging (Fig. 3C). We hypothesized that the FFAT-like domain of ORP3 was activated during mitosis, i.e. phosphorylated to create an acidic-like domain (Weber-Boyvat et al., 2015), and that the post-translational modification of ORP3 in mitosis was due at least in

part to phosphorylation. Indeed, a very significant part of the proteome (~30%) is phosphorylated in mitosis. After treatment of cell extracts from synchronized cells with the CIP phosphatase (Fig. 4B), the migration shift of ORP3 was abolished confirming that ORP3 is indeed phosphorylated in mitosis. Considering the important change in migration speed, this suggested that a large number of residues of ORP3 is phosphorylated during mitosis. We used mass-spectrometry to establish a map of phosphorylated residues in ORP3 in synchronized cells. As we expected, the FFAT-like motif itself, as well as several amino acids downstream, were selectively phosphorylated in mitosis (Fig 4C, yellow residues). To investigate further the consequences of ORP3 FFAT-like domain activation by phosphorylation, we constructed a phosphomimetic-mutant of the ORP3 FFAT-like motif on residues corresponding to acidic residues in the canonical FFAT motif, not including serines downstream (Fig. 4D). We then examined the localization of this "phospho-FFAT-like" mutant in transiently-transfected HeLa cells, compared to WT-ORP3 (Fig. 4E, F). As we expected, this mutant was more strongly localized to the ER than WT-ORP3 even in interphase, particularly around the nuclear membrane and in the vicinity of the Golgi apparatus where ER is abundant. As we often observed in transient ORP3 transfections, the localization of mutated ORP3 to the plasma membrane was also enhanced, suggesting that a very significant part of ORP3 is then located at ER-plasma membrane contacts. Transfected cells were not performed to engage into mitosis and died rapidly, suggesting that ORP3 recruitement to contact sites needs to be finely regulated in the cell cycle. To confirm that ORP3 localization to the ER of the phospho-FFAT-like mutant was mediated by VAPA, we transfected VAPA-KO Hela cells with this mutant (Fig. 4G, H). As expected, the ER localization of the phospho-FFAT-like mutant was strongly decreased – but not fully abolished. It is possible that some of the protein, which has a higher affinity for VAPs, is recruited by VAPB, the less abundant VAP in HeLa cells. From Figures 3 and 4, we conclude that the ORP3 FFAT-like motif is phosphorylated in mitosis and that its phosphorylation enhances recruitment of ORP3 by VAPA to the ER as seen by live-cell imaging between prophase and cytokinesis.

ORP3 regulates PI4P and PI(4,5)P2 at the plasma membrane in mitosis

To better understand the molecular mechanism behind the multinucleated phenotype of ORP3-KO cells, we studied the contribution of ORP3 to PI4P, its transported substrate and PI(4,5)P2, which it is binding at the plasma membrane. Compared to interphase, it is well established that PI(4,5)P2 strongly accumulates at the plasma membrane in mitosis (Roubinet et al., 2011). In addition, PI(4,5)P2 distribution varies at different stages of cell division, with a relative accumulation at the furrow between anaphase and cytokinesis, in order to facilitate the recruitment of actin for ingression of the furrow (Logan et Mandato 2006; Cauvin et Echard 2015). The fluorescent signal appeared much stronger in mitosis from metaphase to late anaphase (Fig. 5A) than in interphase (not shown). In cells stably expressing a PI(4,5)P2 probe (mCherry-PH-PLCδ), the PI(4,5)P2 signal was homogeneous along the cell cortex in metaphase, but there was a progressive increase of the relative PI(4,5)P2 signal at the ingression furrow from metaphase to late cytokinesis (Fig. 5A,B). in WT HeLa cells, a 60% increase in the PI(4,5)P2 signal was measured at the furrow (corresponding to x-axis position 25 and 75 along the cell contour, Fig. 5B, grey line) compared to the poles (Fig. 5B, grey baseline) (Fig. 5C, grey bar). Several phenotypes were observed in ORP3-KO cells. In some cells, the PI(4,5)P2 distribution was asymmetric at the furrow (Fig. 5Aa, b). In other cells, the PI(4,5)P2 increase was more diffuse than just the furrow (Fig. 5Ab), in many cases, the two future daughter cells were slightly asymmetric (Fig. 5 Ab). In ORP3-KO cells, the PI(4,5)P2 fluorescence signal was very strong at the plasma membrane, but the ratio of PI(4,5)P2 at the furrow to the poles culminated at only 30% in cytokinesis (Figs. 5B, 5C green line and bar). The PI(4,5)P2 intensity peaks at the furrow in cytokinesis were also broader in ORP3-KO cells, suggesting impaired PI(4,5)P2 accumulation at the ingression furrow. Due to inter-cellular differences expression levels of the PH-PLCδ probe and signal intensity in non-clonal cell lines, the absolute PI(4,5)P2 concentration cannot reliably be measured and compared between the two conditions. Nevertheless, our results demonstrate that ORP3 deletion results in impaired PI(4,5)P2 distribution at the plasma membrane during mitosis and altered symmetry of the equatorial plane at the onset of cytokinesis. In HeLa cells expressing WT ORP3, PI4P was not particularly enriched at the plasma membrane during early mitosis (not shown). This is consistent with the strong activation of PI4P-5 kinases, which convert most PI4P into PI(4,5)P2 (Roubinet et al., 2011). However, later in mitosis, a stronger signal was observed at the cytoplasmic bridge and even more so at the midbody in WT cells (Fig. 5D, top), where ORP3 is also particularly abundant (see Fig. 3A, bottom inset). Cells

overexpressing ORP3-ΔORD - unable to extract PI4P from the plasma membrane - presented a dramatic increase of PI4P signal all along the cytoplasmic bridge (Fig. 5D, bottom). This phenotype demonstrates the requirement for ORP3 PI4P transfer function, to extract PI4P at the bridge for abscission. Accordingly, it is established that abscission requires PI(4,5)P2 depletion at the bridge by the OCRL phosphatase, to complete abscission (Dambournet et al., 2011). Since OCRL catalyzes the hydrolysis of PI(4,5)P2 into PI4P, our results are consistent with the hypothesis that PIP4 extraction from the membrane is then required to drain both PI(4,5)P2 and PI4P from the plasma membrane in order to complete the abscission.

Cortical actin and the mitotic spindle are dramatically altered in ORP3-KO cells during mitosis

In view of the alterations in PI(4,5)P2 distribution at the plasma membrane in ORP3-KO cells, we then investigated the consequences of ORP3 deletion on the actin cytoskeleton, which is heavily dependent on PI(4,5)P2, in mitosis. Actin staining intensity at the cell cortex was measured in live-cell imaging using spinning-disk microscopy and the SiR-actin probe at different stages of mitosis (Fig. 6A). Unlike the PH-PLCδ probe used to label PI(4,5)P2, this biochemical actin probe turned out to provide a very reproducible intensity readout in each of the two conditions and the actin staining was much more intense in ORP3-KO cells. The average cortical actin intensity signal was therefore measured and compared between WT and ORP3-KO cells (Fig. 6B). A striking and very significative ~4 fold increase in cortical actin was observed in ORP3-KO cells compared to controls at every stage of mitosis from prophase to telophase. This is demonstrating that a dramatic thickening of cortical actin in mitosis occurs at the plasma membrane in the absence of ORP3, consistent with an overall upregulation of PI(4,5)P2. Like for PI(4,5)P2, the actin intensity profile along the cell cortex was measured in cytokinesis (Fig. 6C). In addition, to markedly elevated average actin intensity, the accumulation of actin at the ingression furrow (relative positions 25 and 75, poles at position 0 and 100) was even more strinkingly upregulated in ORP3-KO HeLa cells, compared to WT cells. From our results on PI(4,5)P2 and actin distribution, we propose that ORP3 deletion results in abnormal PI(4,5)P2 accumulation and distribution at the plasma membrane, resulting in a massive increase in cortical actin recruitment an aberrant F-actin cytoskeleton organization in mitosis. PI(4,5)P2 and cortical actin are also know to be important determinants of the assembly and positioning of the mitotic spindle. Using SIR-

tubulin staining of microtubules by spinning-disk microscopy and live cell imaging, we investigated the morphology of the spindle after its assembly in metaphase (Fig. 6D). A statistical analysis of the spindle length and width (Fig. 6D horizontal et vertical dotted lines respectively) revealed that the spindle width was reduced in ORP3-KO cells compared to WT cells, whereas no difference was detected in spindle length (Figs. 6E, 6F). Thus ORP3 deletion, in addition to abnormal cortical actin distribution, results in abnormal spindle morphology. This is likely to account for the various chromosome segregation defects that we observed in ORP3-KO HeLa cells. We hypothesize that the spindle morphology defect could be a result of altered cortical stiffness through F-actin accumulation as previously proposed (Roubinet et al., 2011).

DISCUSSION

Direct lipid transfer of specific lipids, such as phosphoinositides, cholesterol, or phosphatidylserine at membrane contact sites have emerged as a key mechanism to set and regulate the properties and identity of membrane organelles. These lipids often need to be transported against their natural gradient, from the site of synthesis (mostly the ER), where they are present at low concentrations, to their final site of accumulation (Chung et al., 2015; Weber-Boyvat et al., 2015; Mesmin et al., 2017). Counter-transport along its natural gradient of concentration of a different species of lipids, such PI4P, is used by many lipid transfer proteins as a driving force. In most cases, this lipid is also the target of the membrane binding domain of the lipid transfer protein; PI4P in the case of ORP5, ORP8 and OSBP (Mesmin et al., 2013; Moser von Filseck et al., 2014; Antonny et al., 2018), or PA in the case of Nir2 (Kim et al., 2015). In that respect, ORP3 stands out as an exception: it transports PI4P but it binds primarily PI(4,5)P2 (D'Souza et al., 2020; Gulyás et al., 2020). Also, unlike for many other lipid transfer proteins, the counter-transported lipid, phosphatidylcholine, (D'Souza et al., 2020) is much more abundant than PI4P. This suggests that ORP3 function and regulation need to be investigated under a new perspective: instead of using PI4P as a driving force for a counter-transport, ORP3 is likely to deplete membranes from PI4P, when located at contact sites.

In the present work, we further propose that ORP3, in concert with kinases and phosphatases, regulates PI(4,5)P2 at the plasma membrane. The PH domain of ORP3 acts as a PI(4,5)P2

sensor (Fig. 7). In interphase, ORP3 is only weakly and transiently associated with the ER, through its canonical FFAT motif, and with the plasma membrane through its PI(4,5)P2 recognition PH domain (Fig. 7, top). As previously proposed, ORP3 function can be activated by transient post-translational modifications in response to R-Ras and/or PLC signaling, which also affect PI(4,5)P2 at the plasma membrane (Weber-Boyvat et al., 2015). In mitosis (Fig. 7, middle panel), the non-canonical FFAT-like domain of ORP3 is phosphorylated and activated, which results in enhanced ORP3 association with VAPA at the ER. In addition, plasma membrane PI(4,5)P2 levels are elevated, also increasing plasma membrane association of ORP3. We propose that this results in "priming" of ORP3 at ER-plasma membrane contacts for PI4P and PI(4,5)P2 regulation membrane by kinases and phosphatases. In mitosis, PI4P-5K are strongly activated and it is established that differential distribution of kinases and phosphatases contribute to PI(4,5)P2 spatial organization (Roubinet et al., 2011). We propose that constitutive extraction by ORP3 of their PI4P substrate could contribute to the regulation of PI(4,5)P2 accumulation at the plasma membrane. Whether differential ER-plasma membrane contact site spatial distribution in mitosis could also be important remains to be investigated. In any case, our results suggest that ORP3 function is necessary all along mitosis to maintain the PI(4,5)P2 distribution at the dividing cell poles and ingression furrow. As a result, in the absence of ORP3 a dramatic increase in cortical actin is observed all along the plasma membrane and even more so at the ingression furrow. Abnormal stiffening of the cell cortex due to increased F-actin was previously reported to impair cell elongation, contractility and induce defects in the assembly and positioning of the microtubule mitotic spindle in mitosis (Roubinet et al., 2011). Interestingly, we found that the shape of the spindle was altered in ORP3-KO cells. In metaphase, the length of the spindle was normal, but its width was significantly reduced. It is generally believed that spindle length and width are coupled and that this scaling contributes to silencing of the spindle assembly checkpoint (Hara and Kimura, 2013; Chen and Liu, 2016), which underscores the importance of the spindle geometry for cell division. Consistent with our observations of delayed mitosis, the spindle organization defect that we observed is thus likely to delay the spindle assembly checkpoint in ORP3-KO cells. Interestingly, it was recently proposed that spindle width is a better readout of spindle volume than spindle length (Kletter *et al.*, 2022). This suggests that the volume of the spindle is decreased in ORP3-KO cells, which could certainly contribute to the various

chromosome segregation defects that are observed in ORP3-KO cells. It would be interesting to investigate further cell and spindle elongation later in mitosis.

Finally, ORP3 function appears to be absolutely essential to drain PI4P from the cytoplasmic bridge at the end of cytokinesis, before abscission (Fig. 7, bottom). Accordingly, it is well established that the OCRL phosphatase is required to convert PI(4,5)P2 into PI4P and to lower PI(4,5)P2 levels at the bridge (Carim et al., 2019). This step is key for releasing the actin cytoskeleton and to permitting the recruitment of ESCRT complex for abscission. We found that in the absence of a functional ORP3 protein, PI4P dramatically accumulates at the cytoplasmic bridge and restricts PI(4,5)P2 depletion. To our knowledge, ER-plasma membrane contact sites, where ORP3 could function, were never described at the cytoplasmic bridge. However, the accumulation of ORP3 at the midbody in WT cells strongly supports that it functions at this location in cytokinesis. In the absence of ORP3, we see elevated PI4P levels at the bridge, which is likely delay or impair abscission. Indeed, abscission failure and daughter cell re-fusion after mitosis is one of the phenotype that we observed in ORP3-KO cells.

In conclusion, beyond previsouly described ORP3 role in interphasic cells in response to cell signaling, the transport of PI4P by ORP3 is essential to participate in the exquisite regulation of PI(4,5)P2 and PI4P at different plasma membrane domains all along mitosis.

ACKNOWLEDGMENTS

We warmly thank Arnaud Echard, Katja Wassmann, Fabien Alpy, Phong Tran and the past and current members of the Membrane Dynamics and Intracellular Trafficking team at Institut Jacques Monod for insightful discussions. We acknowledge the ImagoSeine core facility of the Institut Jacques Monod of IBiSA and France BioImaging (ANR-10-INBS-04) infrastructures, for flow cytometry, light microscopy, and electron microscopy. This work was supported by grants from the Ecole doctorale Bio Sorbonne Paris Cité and the Labex “Who Am I” (A.V), the Agence Nationale de la Recherche (ANR 225916 EndoMitR and ANR 237213 SynaptoLigation), the Ligue Contre le Cancer (RS21/75-85).

MATERIALS AND METHODS

Cell culture

Hela cell lines were cultured in Dulbecco's modified Eagle's medium (DMEM) 1g/L D-glucose medium (Gibco), supplemented with 10% fetal bovine serum (Gibco) and 100 units/ml penicillin (Gibco), in 5% CO_2 at 37°C. HeLa AP cells were edited with a double nickase strategy to generate the CRISPR control and VAPA KO cell lines using (Siegfried et al., 2024). HeLa AP cells were edited with a single nickase strategy to generate the CRISPR control and ORP3 KO cell lines (cf "Cell line editing using CRISPR/Cas9" section). All stable HeLa AP cells lines (ORP3 KO-rescues) were grown in DMEM 1g/L D-glucose medium, supplemented with 250 units/ml Geneticin G418 (Gibco).

Cell transfection

Cells were transfected with Lipofectamine™ (Thermofisher). DNA Plasmid transfection was performed using Lipofectamine™ 2000 (Thermofisher), according to manufacturer's recommandations. HeLa cells were transfected at a 60-70% confluence. For transfection, 1 µg plasmidic DNA was resuspended in 100µl OPTI MEM (1X) + GlutaMAX™-I media (Gibco). 3µl lipofectamine 2000 were resuspended in 100µl OPTI MEM. Resuspended DNA and lipofecamine 2000 were mixed for 10 min, then homogenized with the cell medium for transfection. 4h after transfection, the medium was replaced with DMEM 10% supplemented with 10% FBS. Cells were imaged the next day. siRNA plasmid transfection was performed with Lipofectamine™ 3000 (Thermofisher) according to manufacturer's instructions. HeLa cells were transfected at a 50-60% confluence. 2µg siRNA were used for 5µl of lipofectamine 3000. 2µg of siRNA were first resuspended in 200µl OPTI MEM (1X) + GlutaMAX™-I media. 5µl lipofectamine 3000 was resuspended in 200µl OPTI MEM. Resuspended DNA and lipofecamine 2000 were mixed for 10 min, then homogenized with the cell medium for transfection. Cells were incubated overnight in the transfection medium. The medium was then replaced with DMEM containing FBS. Cells were imaged three days after transfection.

Probes for live-cell imaging

Fluorescent probes were used to stain cell compartments for live-cell imaging. The probes were diluted as much as possible to prevent interference with cell viability. SiR-DNA (λ674)

(Spirochrome) and Spy-DNA (λ505) (Spirochrome) were prepared with 0,4 nM verapamil enhancer according to manufacturer's instructions. They were diluted 1:2500 in FluoroBrite™ DMEM supplemented with 10% fetal bovine serum and 100 units/ml penicillin OPTI MEM. SiR-Actin (λ674) and Spy-Tubulin (λ505) were used at a 1:5000 dilution.

Antibodies

Primary antibodies used for immunofluorescence: anti-ORP3 rabbit IgG polyclonal (1:300, Abcam, 224212); anti-PI4P mouse IgM monoclonal (1:200, Echelon Biosciences, Z-P004); anti-PI(4,5)P2 mouse IgM monoclonal (1:200, Echelon Biosciences, Z-P045). Secondary antibodies used for immunofluorescence: Alexa Fluor™ 488 Goat anti-Mouse IgG polyclonal (1:10000, Invitrogen, A11001); Alexa Fluor™ 488 Goat anti-Rabbit IgG polyclonal (1:10.000, Invitrogen, A11034); Alexa Fluor™ 555 Goat anti-Mouse IgM polyclonal (1:10.000, Invitrogen, A21426). Primary antibodies used for the western-blotting: anti-ORP3 mouse IgG monoclonal (1:1000, Santa Cruz Biotechnology, sc-398326); anti-VAPA rabbit polyclonal (1:1000, Atlas Antibodies, HPA009174); anti-GAPDH mouse IgG monoclonal (1:2000, GeneTex, GTX627408); anti α-tubulin mouse IgG monoclonal (1:1000, GeneTex, GTX628802). Secondary antibodies used for western-blotting: Peroxidase anti-mouse IgG sheep monoclonal (1:10.000, GE Healthcare UK, LNA931V/AH); Peroxidase anti-rabbit IgG rat polyclonal (1:10.000, Jackson Immuno-research, 312-006-045).

Plasmids

All the plasmids used have been sequence using the service plasmidsaurus. The ORP3 plasmid was a gift from the Olkkonen team, and corresponds to the full-length human ORP3 isoform 1a 887 amino acids (Lehto et al., 2005). We produced a collection of ORP3 mutants by editing this plasmid. All ORP3 plasmid exhibit kanamycin resistance and harbor either enhanced GFP (GFP) or mCherry N-terminal tags. The GFP-ORP3 Δ-PH mutant was generated using a synthetic gene, with a deletion of aa 51-145 aa of ORP3 corresponding to the PH domain, and cloned using HindIII/ Bbsi insertion sites. The GFP-ORP3 FFAT^{m} plasmid, with mutations in the FFAT motif (EFFDAQE → EVVAAQE) was generated by PCR mutagenesis, and inserted using restrictions enzymes EcoNI/XagI. The GFP-ORP3 FFAT-like^{m} plasmid, with mutations in the FFAT-like motif of ORP3 (HFFSGST → HVVAGST) was generated by PCR and inserted in the ORP3 plasmid by enzyme restriction

HindIII/BbsI. The GFP-ORP3 FFAT-like^{m} and FFAT^{m} double mutant plasmid were generated by PCR and inserted using BbsI and Kpn1 enzymes. Likewise, the GFP-ORP3 FFAT-like phosphor-mimetic and GFP-ORP3 ΔORD mutants were generated by PCR. The GFP-ORP3 ΔDLSK mutant was generated by insertion of a synthetic sequence of the ORD domain depleted for the sequence gacctgtccaag (DLSK), and cloned using enzymatic restriction with BbsI/AflII.

PCR mutagenesis was performed accordingly to the following templates. Presentation from 5' to 3' (capital letters indicating mutations). Plasmid p-ORP3-FFAT^{m} (5' gactccctttctgagGtGGttgCtgctcaggaagttctgttatctccaag 3'), plasmid p-ORP3-FFAT-like^{m} (5' tccacatgaagttaaccacGtGGtGGcCgggtccaccatcacagactcttcatc 3'), plasmid p-ORP3-FFAT-like-phospho-mimetic (5' catgaagttaaccactttttcGACggAtccGATatcacagact -cttcatctgg 3'), plasmid p-ORP3-Δ-ORD (5' catctgaGAATTCAACATCCTGAGGAACA -ACATCGG 3'). The mCherry-VAPA and mCherry-VAPA$^{KD/MD}$ plasmids were generous gifts from Fabien Alpy (IGBMC, Illkirch). The GFP-VAPB and GFP-P4M-SidM probe plasmids were obtained from Addgene (respectively #108126 and # 514711). GFP-PH-PLCδ was a kind gift from Francesca Giordano (I2BC, Gif-sur-Yvette). The GFP-Mapper probe was a gift from Jen Liou (UT Southwest Medical Center, Dallas), also available as Addgene plasmid #117721. RFP-KDEL was a gift from Nihal Altan-Bonnet (NHLBI, Bethesda).

Silencing ORP3 by RNA interference (siRNA)

The siRNA sequences target the endogenous mRNA on the 5' end, upstream of the ORP3 PH domain, absent in the plasmid sequence synthesized by Eurofins. The absence of off-targets was verified using BLAST.

ORP3 siRNA 1	5' - ccuugauaguggucgggaatt -3'
mock ORP3 siRNA 1	5' - gugcagauugacggcuagutt -3'
ORP3 siRNA 2	5' - gcuuucuaaugaaaguagatt -3'
mock ORP3 siRNA 2	5' - agaacuauugaucguaaugtt -3'

Note: The ORP3 siRNA 1 and mock ORP3 siRNA were previously used by Letho *et al.,* (Lehto et al., 2005).

Cell line editing with CRISPR/Cas9

The HeLa AP CRISPR-Cas9 ORP3-KO cell line was generated using a GFP single nickase ORP-3 CRISPR/Cas9 KO Plasmid (Santa Cruz), containing a pool of the three following guide RNA (gRNA):

gRNA 1 5'-gggggagatgaattacaccc -3'

gRNA 2 5'-tacctgtcgacttccttgct -3'

gRNA 3 5'-atgcatagaccttgacaccg -3'

These gRNA are targeting sequences in the mRNA sequence of ORP3 prior to the start codon of the wild type isoform. The control plasmids contain scrambled guide RNA, with no detectable off target in humans using BLAST. The cells were transfected with either the ORP3 CRISPR/Cas9 plasmid, or the control plasmid using Lipofectamine 2000 (Thermofisher). Due to the absence of antibiotic resistance in the plasmid, positive clonal cell lines were isolated by FACS using the GFP signal. The clones were further screened by western blotting for negative ORP3 protein signature. A secondary screen was performed to check the absence of GFP signature. The ORP3-KO stable cell lines were used to generate stable rescue cell lines expressing wild-type GFP-ORP3 or mutants (cf “Plasmids” section). Stable clones were sorted by FACS and verified by western blotting and fluorescence microscopy. VAPA KO cell lines were generated by CRISPR/Cas9 using double nickase plasmids (Santa Cruz, sc-424440-NIC) and controls (Santa Cruz, sc-437281), as previously described in Caco-2 cells (Siegfried et al., 2024). The mCherry-PH-PLCδ and mCherry-P4MSidM stable cell lines were generated in three different backgrounds: HeLa AP wild type cell lines, mock ORP3 KO cell lines and ORP3 KO cell lines and sorted to generate clonal populations using FACS. The cell lines were verified by western blotting and microscopy.

Cell synchronization

The protocol used for prometaphase synchronization was described in (Zieve et al., 1980). The cells were seeded to reach 80% confluency on the first day of treatment. Cells were treated with thymidine 2mM (Merck KGaA) for 24h, to ensure blocking in S-phase. The thymidine block was released by a 3h Phosphate Buffered Saline (PBS, Glibco) wash, to allow cell-cycle progression to prophase. 100 ng/ml Nocodazole (Merck KGaA) was added to the culture medium for 12h to ensure the mitotic block in prometaphase. The block was then released by PBS wash, allowing cell progression through mitosis.

Western blotting

Cells were grown to confluence in 6-well dishes (TPP) and washed 3 times with PBS. Cells were lysed using 200µl lysis buffer 50 mM Tris pH 8.5 (CarloErba SDS, 1560517), 150 mM NaCl (MERCK, 1.06404.1000), 1X protease inhibitor cocktail with EDTA (Roche, 05056489001), 0.5% triton-X100 (Sigma, T9284-100ML) for 10 min at 4°C on ice. Lysates were centrifuged for 20 min at 4°C at 13000 g, and supernatants were collected without the insoluble fraction. Protein concentrations were quantified in 96-well plate (TPP) using a Spectramax imager, by the Bradford assay (BioRad). Samples of 20µg total protein contents in SDS-PAGE loading buffer (Fermentas, R0891). Protein denaturation was performed at 95°C for 10 min. The PageRuler Plus Prestained Protein Ladder (Thermoscientific, 26619) was used as a size reference. Electrophoresis was performed on 4-12% Mini-PROTEAN TGX Stain-Free Precast Gels (Bio-Rad) in running buffer with tris 25mM, glycine 0.192M (MERCK, 10421025), SDS 0.1% (Euromedex, Eu0660) at 200V; and transferred on 0.45µm pore PVDF membranes (Amersham Hybond, GE10600023) in transfer buffer containing tris 25mM, glycine 192mM, pure ethanol 20% (VWR, 20824.365) at 400mA. Before antibody hybridization, membrane blocking was performed with 5% skimmed dry milk (Régilait) in PBS containing 0.1% Tween 20 (Biosolve, 20452335). Primary antibodies were incubated in wstern buffer and incubated overnight at 4°C. After three washes with the western buffer, secondary HRP antibodies were diluted in western buffer and incubated for 1 hour, then washed three times with western buffer. Antibodies were detected using the Supersignal west femto maximum sensitivity substrate (Amersham, KB011) and visualized with a ChemiDoc chemiluminescence detection system (Bio Rad). Quantification of western blots was performed by densitometry by comparing the band of interest with a housekeeping gene. Quantification was performed using the Gel analyzer plugin of Fiji imaging software (version 2.16.0).

Immunoprecipitation

HeLa cells were seeded the day before the experiment, then lysed (cf “Western blotting" section). The cell lysates were incubated overnight in with IgG Sepharose beads (GE Healthcare, 17-0969-01) coated with anti-VAPA primary antibodies (cf “Antibodies” section).

After 5 washes with lysate buffer, anti-VAPA bound proteins were denatured 10 min at 95°C, and subsequently loaded for western blotting.

CIP dephosphorylation

HeLa cells were seeded the day before the experiment and synchronized (cf "Cell Synchronization" section). After lysis, the proteins supernatant was treated with CIP phosophatase for 1 hour.

Confocal fluorescence microscopy

Fluorescence microscopy imaging was performed using a Yokogawa CSU-X1 Spinning Disk confocal mounted on an inverted motorized Axio Observer Z1 (Zeiss) and equipped with a sCMOS PRIME 95 (photometrics) camera and a 63X oil-immersion objective (1.4 numerical aperture). The laser (GATACA Systems, I launch) power was set to a constant 15% for all the wavelengths of interest. Z-stacks images were acquired at a z-resolution of 2 µm for all acquisitions, excepted for the tubulin imaging where z-resolution was set at 0.5 µm. For live-cell experiments, microscopy was performed in a closed chamber set to 37°C under 5% CO_2 atmosphere. Images were acquired using the MetaMorph software (Version 7.10.5.476). For microscopy, cells were grown on segmented IBIDI µ-Dish 35 mm (IBIDI), to ensure simultaneous and identical imaging conditions for the different experimental conditions. 90 min before imaging, sample's media were changed for FluoroBrite™ DMEM, supplemented with 10% fetal bovine serum and 100 units/ml of penicillin. Depending on the experiment, this media was completed with fluorescence fluorescent DNA, tubulin or actin probe (Spirochorme, cf "Probes for live-cell imaging" section). To limit the impact of phototoxicity, movies were acquired for 2 hours only with a time resolution of 3 min. Image processing and analysis were carried out using Fiji imaging software.

Immunofluorescence microscopy

Cells were seeded on 18mm diameter glass coverslips (#1.5, VWR, 631-0153) at 60% confluency. The next day, cells were washed with PBS. For formaldehyde fixation (Thermo scientific, 28908), cells were fixed in a 4% formaldehyde diluted in PBS for 15 min at room temperature. For methanol fixation (VWR, 20847.295), cells were fixed using pre-chilled methanol (-20°C) for 15 min. Cells were then washed 3 times with NH4Cl 50mM (VWR,

21236.291) in PBS, then incubated in permeabilizing solution containing 0,5% Bovine Serum Albumin (BSA, Sigma, A3059-100G) and 0,1% Triton (Sigma, T9284-100ML) in PBS for 15 min. Cells were incubated with primary antibodies diluted in the incubation solution for 1 hour at room temperature. Samples were washed 3 times using the permeabilizing solution. Cells were next incubated with the secondary antibodies for 1 hour at room temperature used in the permeabilizing solution with cross-adsorbed Alexa 488 and Alexa 555 anti-mouse/anti-rabbit IgG secondary antibodies (cf antibody section) and washed in PBS. Cells were labelled with DAPI (Sigma Aldrich, ref: D9542) for 5 min in PBS, washed In PBS and mounted on slides using 8µl of VECTASHIELD® Antifade Mounting Medium (Vector laboratories), and sealed using nail polish. Slides were images at confocal Yokogawa CSU-X1 Spinning Disk (cf fluorescent microscopy section).

Electron microscopy

In order to examine the distribution of membrane contact sites between the ER and the plasma membrane, Serial block-face Scanning electron microscopy (SBF-SEM) EM was used. This technique allows 3D imaging of cells and tissues at the ultrastructural level. HeLa Cells were fixed in 3% formaldehyde (Thermo scientific, 28908), 1% glutaraldehyde (Electron microscopy sciences, 16400) during 1 hour at room temperature and prepared for SBF-SEM as previously described (Lachat et al., 2022). For imaging, a TeneoVS SEM (ThermoFisher Scientific) was used with a beam energy of 2.7 kV, 100 pA currents, in LowVac mode at 40 Pa, a dwell time of 1 µs per pixel at 10 nm pixel size. Sections of 100 nm were serially cut between images.

Microscopy Image analysis

The percentage of multinucleated cells within a population was assessed by imaging coverslips fixed with formaldehyde treatment, and stained with DAPI for 5 min before fixation. For each experimental condition, 20 regions of the coverslip were randomly acquired. The ratio of multinucleated/mono-nucleated cells was calculated after using the Fiji cell counter plugging. Only cells fully visible in the 3D-field of view with non-ambiguous nuclei in the different z-stacks were analyzed. Division aberrations and cell division timing were characterized by live imaging of dividing cells stained with SiR-DNA (λ674) probe. The quantification of actin was performed in dividing it by the actin intensity at the cell poles and

clivage furrow in anaphase. Cells were incubated 1 hour before imaging in FluoroBrite™ DMEM (Gibco) supplemented with 10% fetal bovine serum (Gibco), 100 units/ml of penicillin, SiR-DNA (λ674) and Spy-Actin(λ505). PI(4,5)P2 quantification in mitotic cells, was performed by live cell imaging of mCherry-PH-PLCδ stable cell lines. The intensity was measured along the cell contour starting at one pole of the dividing cell. For quantification purposes (averaging between cells), the total length of the cell contour was normalized to 100. The same approach was used to measure actin intensity at the cortex in late mitosis. Colocalization between ORP3 and VAPA, or ORP3 and KDEL was assessed by using the Pearson colocalization module of the Fiji imaging software. Before quantification, images were filtered (Median filter r=1, Gaussian blur r=1). To restrict the localization analysis to the cytosol where both proteins are present, a mask corresponding to ORP3 distribution was created, and added to the colocalization settings. Furrow size was measured on 15 z-stack slides, where z-resolution was set at 0.5µm.

Graphs and statistical analysis

Quantifications were performed using two-tailed Student's t-test assuming equal variances to compare the distributions. * $p < 0.05$; ** $p < 0.01$. *** $p < 10-3$.

The graphs were generated using templates available on bio render.

FIGURES

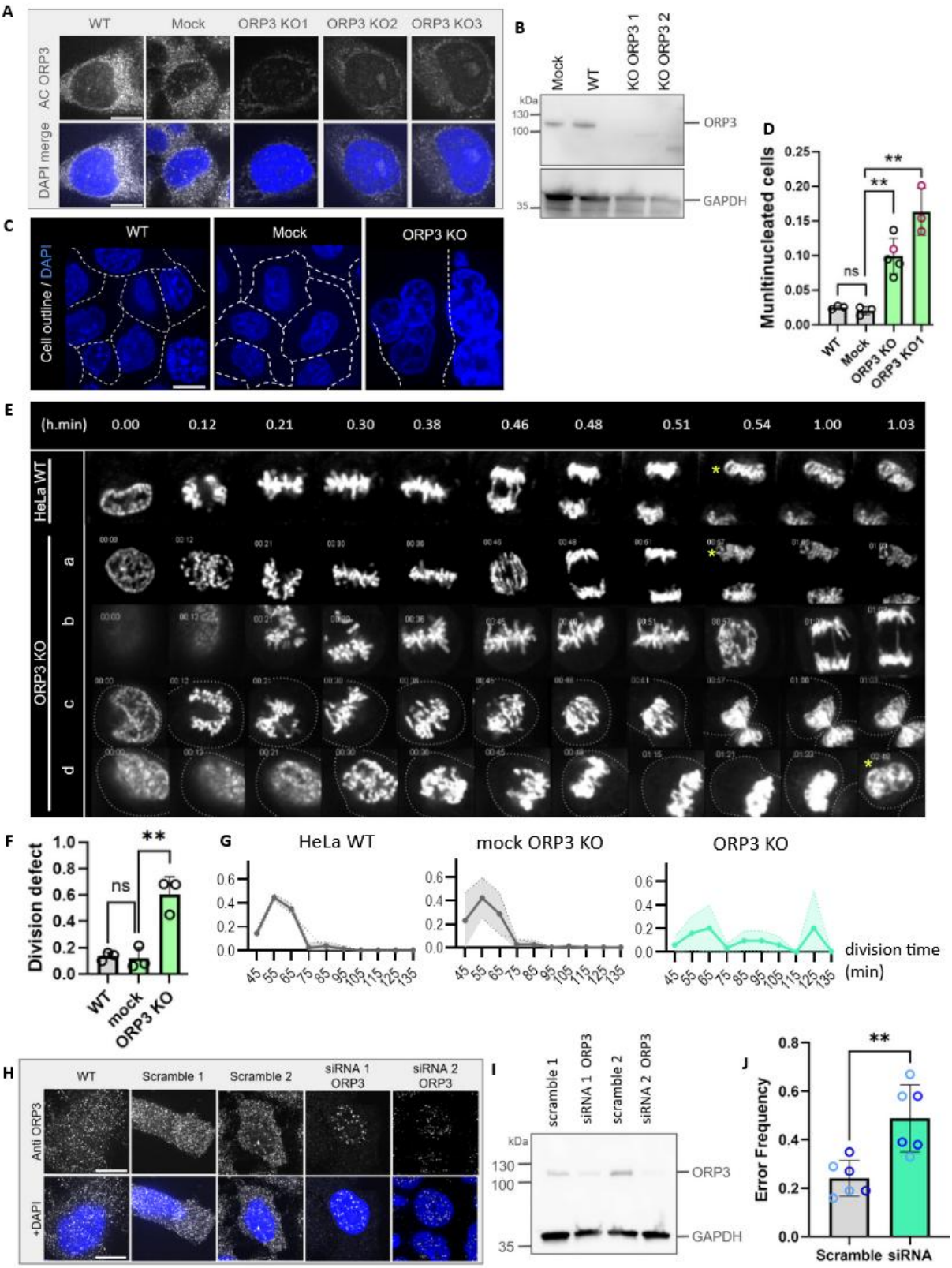
A
WT
Mock
ORP3 KO1
ORP3 KO2
ORP3 KO3
AC ORP3
DAPI merge
B
Mock
WT
KO ORP3 1
KO ORP3 2
kDa
130
100
35
ORP3
GAPDH
C
WT
Mock
ORP3 KO
Cell outline / DAPI
D
Multinucleated cells
ns
**
WT
Mock
ORP3 KO
ORP3 KO1
E
(h.min)
0.00
0.12
0.21
0.30
0.38
0.46
0.48
0.51
0.54
1.00
1.03
HeLa WT
ORP3 KO
a
b
c
d
F
Division defect
ns
**
WT
mock
ORP3 KO
G
HeLa WT
mock ORP3 KO
ORP3 KO
division time (min)
H
WT
Scramble 1
Scramble 2
siRNA 1 ORP3
siRNA 2 ORP3
Anti ORP3
+DAPI
I
scramble 1
siRNA 1 ORP3
scramble 2
siRNA 2 ORP3
kDa
130
100
35
ORP3
GAPDH
J
Error Frequency
**
Scramble
siRNA

Figure 1 - ORP3 is required for proper cell division.

ORP3 was deleted from HeLa cells using CRISPR-Cas9 and several clones were characterized. **A** Immunofluorescence staining with polyclonal anti-ORP3 polyclonal antibodies (white) in clonal cell lines from CRISPR Mock and ORP3-KO (3 distinct clones) HeLa cells. Nuclei were counter-stained with DAPI. Bar: 10 µm. **B** Immunoblot staining for ORP3 from WT and CRISPR Mock or ORP3-KO (clones 1, 2) cells. GAPDH was used as a loading control. **C** In fixed cells stained with DAPI, ORP3-KO cells exhibited an accumulation of multinucleated cells. Clone 1 shown. Bar: 20 µm. **D** Statistical analysis of the fraction of multinucleated cells in WT, Mock (3 distinct clones) and ORP3-KO cells (5 distinct clones). Clone 1 (red circles), was used for the following experiments. **E** Live-cell imaging of mitosis from prophase to cytokinesis in WT HeLa cells (top) and ORP3-KO cells (lines a-d), showing typical ORP3-KO mitotic phenotypes: (a) no defect, (b) lagging chromosomes, (c) no DNA segregation between the two daughter cells and (d) segregation of all the DNA into only one of the daughter cells. DNA was stained with SiR-DNA. **F** Quantification of overall division defects in WT, Mock and ORP3 KO cell lines n=3 experiments. **G** Duration of cell division from nuclear envelope breakdown to the beginning of DNA decondensation in WT, Mock and ORP3-KO cells. Actual acquisition frequency was 3 minutes (10 minutes binning on the graph). N=3, 20-30 cells/experiment. **H** Immunofluorescence staining with anti ORP3 antibodies (white) and DAPI (blue) of WT, scramble siRNA- or ORP3 siRNA-treated HeLa cells. Bar: 10 µm. **I** Immunoblot staining for ORP3 from WT, scramble siRNA or ORP3 siRNA-treated (2 distinct siRNAs) HeLa cells. GAPDH was used as a loading control. **J** Quantification of the division defects in scramble and ORP3 siRNA treated HeLa cells. Light blue: siRNA/Scr1, dark blue: siRNA/Scr2 (n=6).

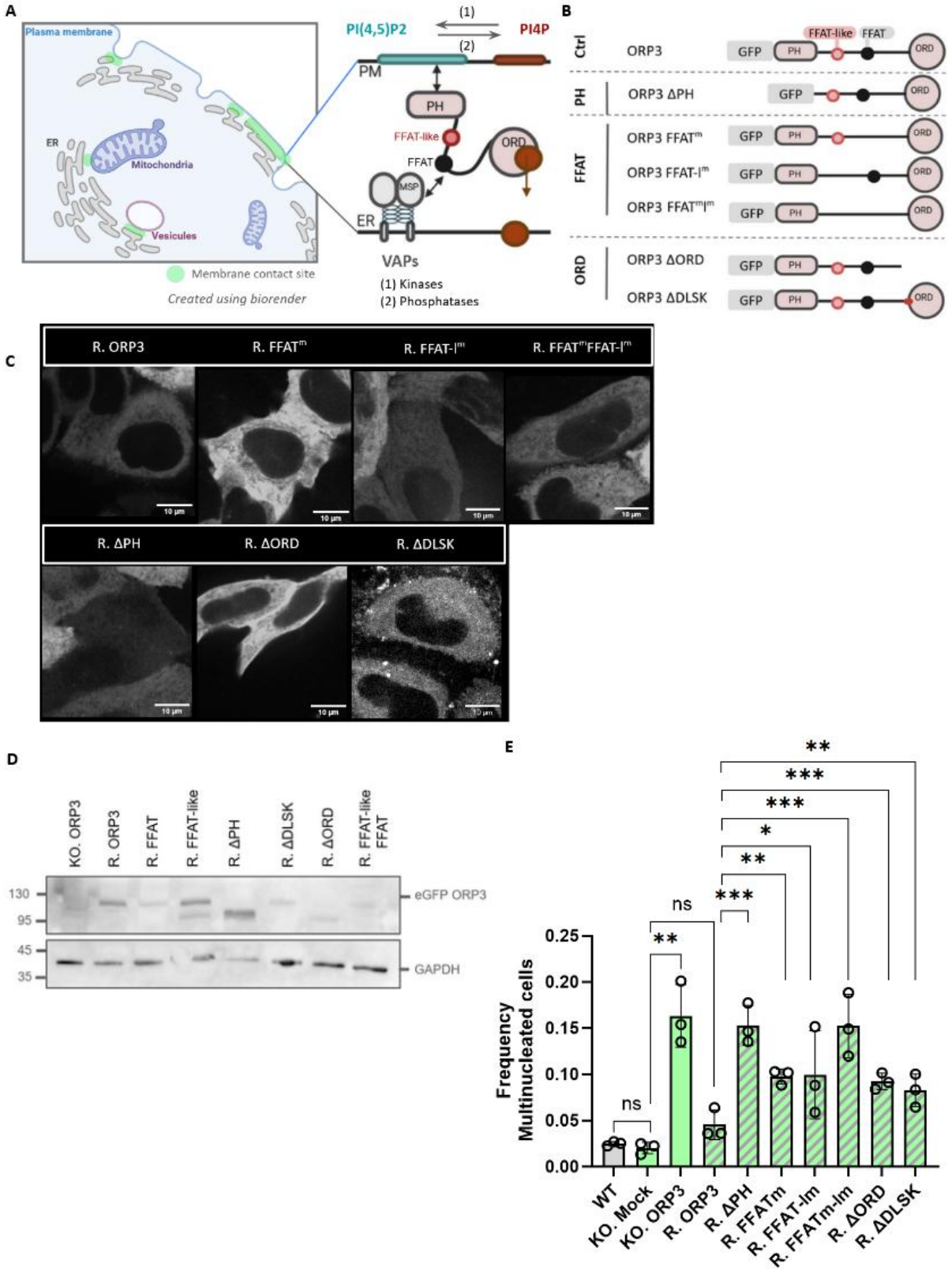

<u>Figure 2 – All the major domains of ORP3 are necessary for its function in mitosis.</u>
A Scheme of ORP3 localization and function at membrane contact sites (light green) between the plasma membrane and the ER. **B** Scheme of the different GFP-ORP3 mutants used for rescue experiments in ORP3-KO HeLa cells. Mutations in the PH and ORD domains were

deletions, whereas FFAT mutations were substitutions in the motif. **C** Localization of ORP3-KO HeLa cells expressing WT-GFP-ORP3 (R. ORP3) and mutants in live cells by spinning disk confocal microscopy. Bar=10µm. **D** Immunoblot staining with anti-ORP3 antibodies in GFP-ORP3 and mutants stably expressed in ORP3-KO HeLa cells. Staining with anti-GAPDH antibodies was used to normalize the ORP3 expression level. As expected, deletion of the PH (Δ1-150) or the ORD (Δ480-887) domain results in a smaller protein. **E** Frequency of multinucleated cells in fixed cells (DAPI-stained) in WT cells, ORP3-KO, Mock and the different rescue cell lines, n=3 experiments for each condition.

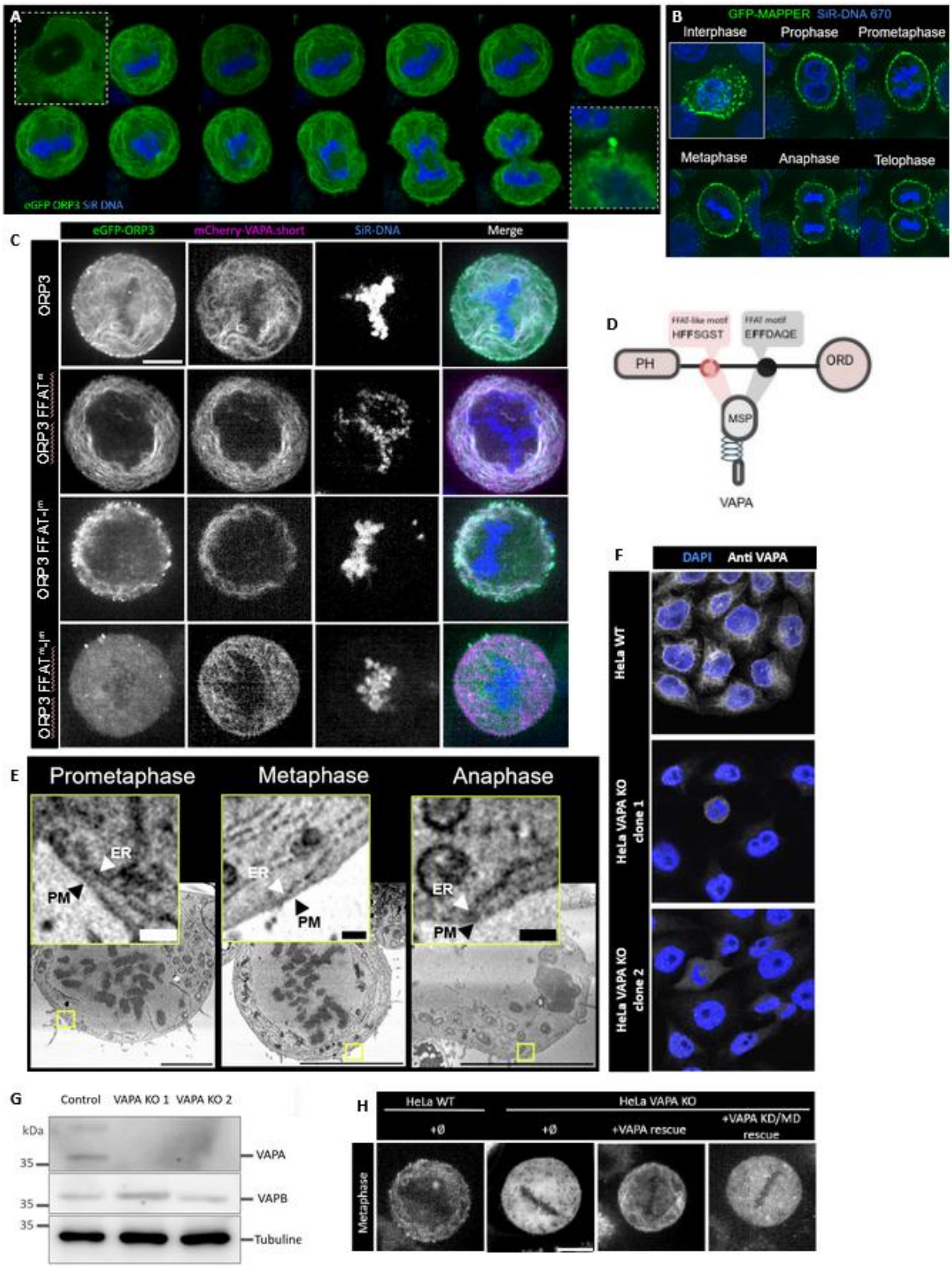

Figure 3 – ORP3 is strongly recruited to the ER by VAPA through both ORP3 FFAT domains.

A Live-cell imaging of stable GFP-ORP3 HeLa cells stained with SiR-DNA during mitosis. Top inset: in interphase, VAPA is mostly cytosolic. ORP3 is recruited to the ER from prophase to telophase, with a final enrichment at the midbody later in abscission (bottom inset). **B** localization of the ER-plasma membrane contact probe GFP-mapper in interphase (inset) and throughtout mitosis. Blue: Sir-DNA staining. **C** FFAT-dependent ER localization of ORP3. In live cell imaging, ORP3-KO HeLa cells stably expressing WT-GFP-ORP3 co-localizes with mCherry-VAPA at the ER. This localization persists if either FFAT (ORP3-FFAT^{m}) or FFAT-like (ORP3-FFAT-like^{m}) are inactivated, but not when both motifs are defective. **D** Detailed scheme of ORP3 FFAT and FFAT-like domain sequence. **E** SBF-SEM electron microscopy of ORP3-KO HeLa cells demonstrates the existence of ER-plasma membrane contacts from metaphase to anaphase even in the absence of ORP3. **F** Anti-VAPA antibody staining in WT HeLa cells and stable VAPA-KO cell lines (white) DNA is stained with DAPI (blue). **G** Western blot of VAPA and VAPB of control and VAPA-KO HeLa cell lines. Only the VAPA signal is abolished in VAPA-KO cells. Tubulin was used as loading control. **H** VAPA-dependent ER localization of ORP3. Live-cell imaging in metaphase of stable GFP-ORP3 in WT-HeLa cells (left) and VAPA-KO HeLa cells (second from left), VAPA-KO cells rescued with WT-VAPA (third from left) or VAPA mutated in its FFAT binding domain (VAPA KD/MD, right). Bar=20µm.

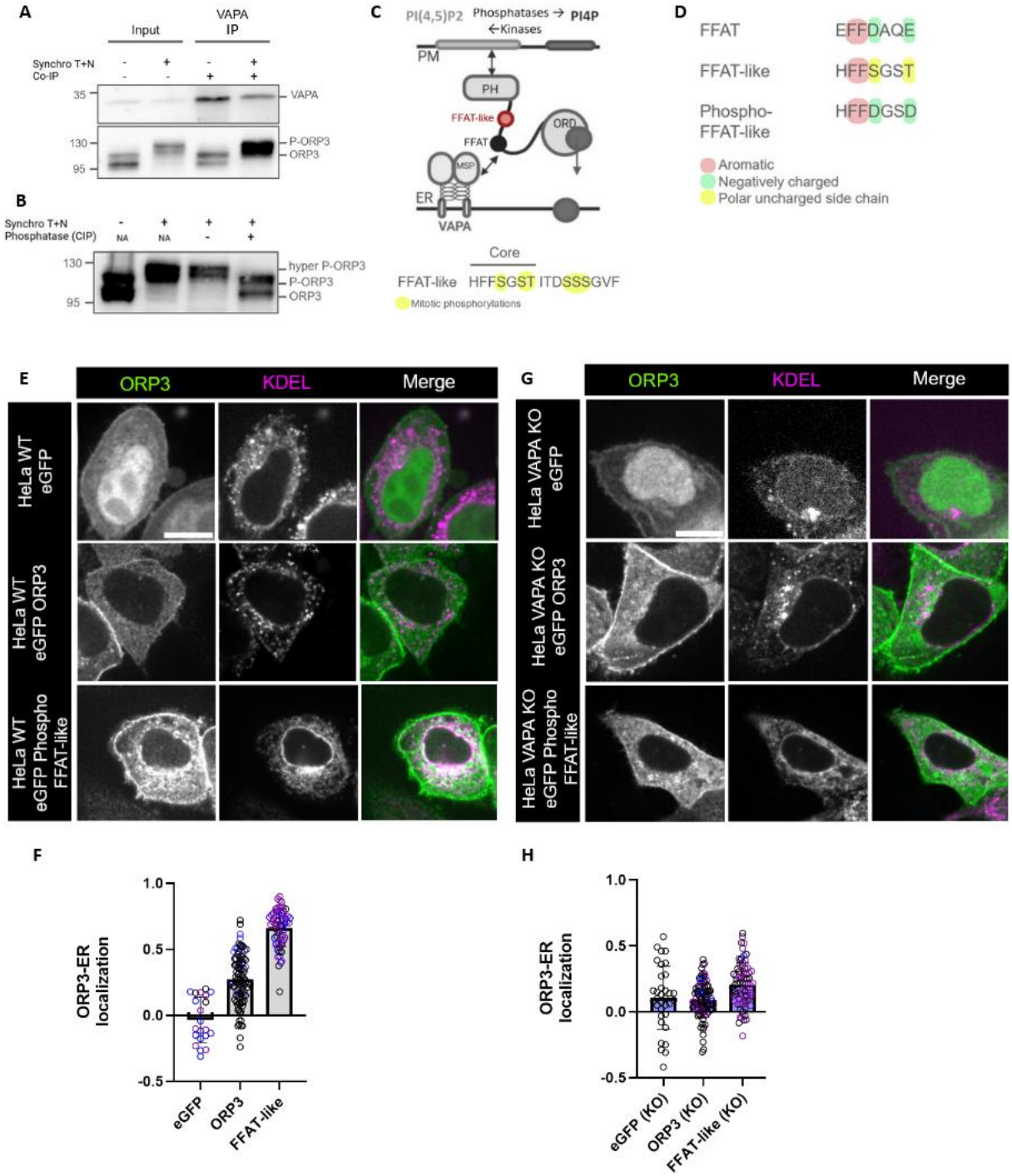

Figure 4 – Phosphorylation of the FFAT-like domain of ORP3 enhances its ER localization.

A VAPA-immunoprecipitation of non-synchronized HeLa cells and cells synchronized by a double thymidine + nocodazole block (T+N). VAPA is detected in the input (left), and after VAP immunoprecipitation (VAPA IP) in both conditions (- or + Synchro T+N). ORP3 is present in the input in comparable amounts but display a migration delay in synchronized cells (Synchro T+N). In T+N synchronized cells, ORP3 immunoprecipitation by VAPAis strongly enhanced. **B** In HeLa cells extracts from synchronized (T+N) or non-synchronized,

treatment with the CIP phosphatase reversed the migration delay of ORP3 in T+N synchronized cells. The left two lanes (NA) were not subject to the enzymatic incubation **C** Scheme of ORP3 and the sequence of its FFAT-like domain (Core) and amino acids downstream. Mass spectrometry has confirmed that many ORP3 residues were phosphorylated in synchronized cells (but not non-synchronized cells), including the three S and T residues of the FFAT-like domain and 3 serines just downstream of it (all highlighted in yellow). **D** Design of a FFAT-like phosphomimetic mutants, where S and T residues in the FFAT-like motif, which correspond to acidic residues in canonical FFAT, are replaced by aspartic acid (D). **E** WT-HeLa cells double-transfected with mCherry-KDEL and GFP, WT-GFP-ORP3 or the phosphomimetic mutant of ORP3-FFAT-like:(GFP-phospho-FFAT-like). Bar=20µm. **F** Quantification of the ER co-localization of GFP alone, GFP-WT-ORP3, and GFP-phosphomimetic mutant (FFAT-like). **G** VAPA-KO HeLa cells double-transfected with mCherry-KDEL and GFP, WT-GFP-ORP3 or the phoshomimetic mutant of ORP3-FFAT-like:(GFP-phospho-FFAT-like). Bar=20µm **- H** Quantification of the ER co-localization of GFP alone, GFP-WT-ORP3, and GFP-phosphomimetic mutant (P-FFAT-like) in VAPA-KO HeLa cells.

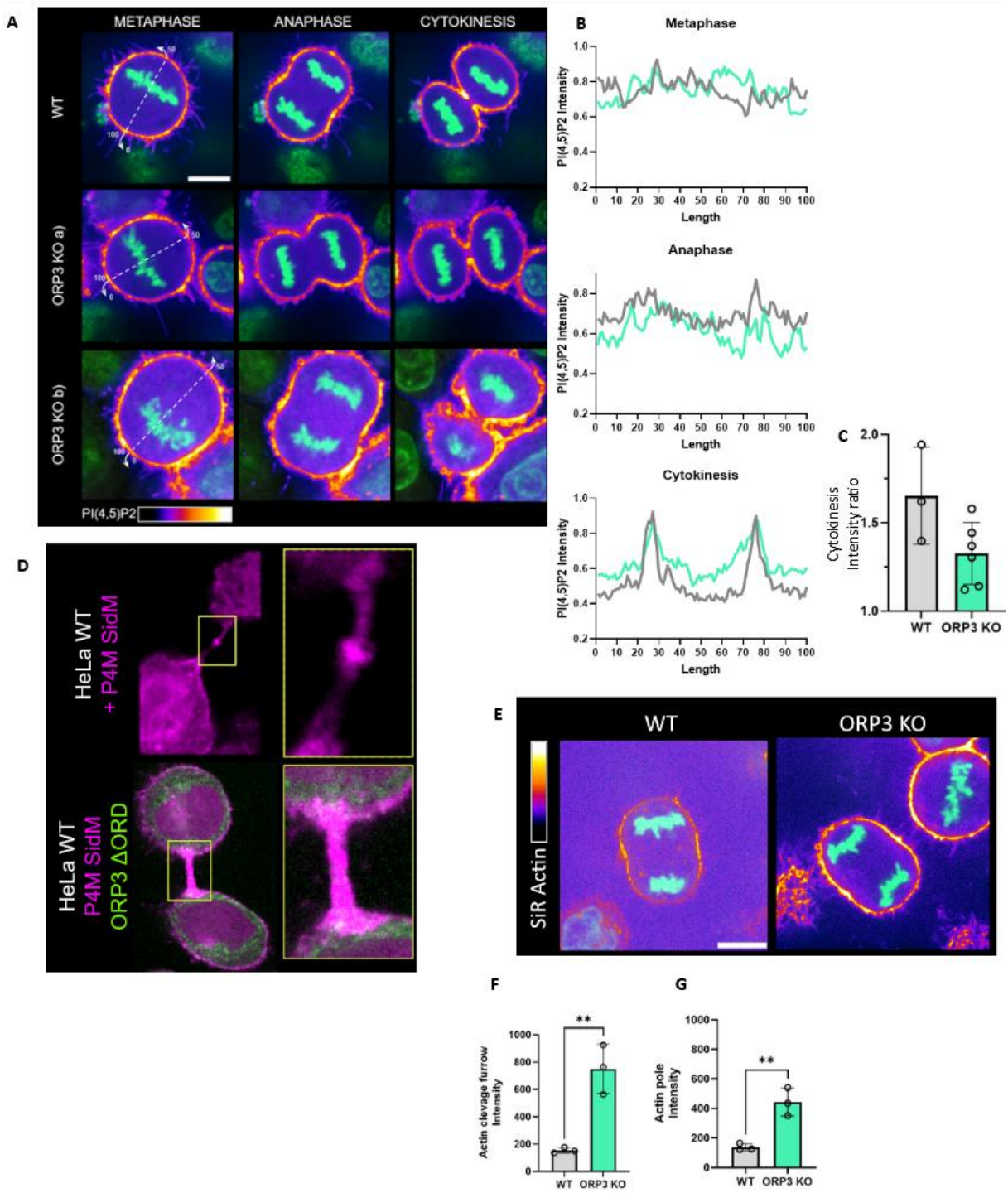

Figure 5 - ORP3 regulates PI4P and PI(4,5)P2distribution at the plasma membrane during mitosis.

A Live cell imaging spinning disk confocal microscopy of PI(4,5)P2 and DNA (SiR DNA 670) at 3 different mitotic stages in WT and ORP3-KO cells stably expressing mCherry-PH-PLCδ. Bar=20µm. PI(4,5)P2 intensity is represented by a heat-map LUT. **B** Quantification of the relative PI(4,5)P2 intensity along the plasma membrane in each of the phases (arbitrary units). Membrane length was normalized with position 0/100 corresponding to one pole and 25 (and 75) to one on the two side of the equatorial plane. **C** Quantification of PI(4,5)P2 in-

tensity at the furrow in cytokinesis compared to the poles. n=2 experiments, each dot corresponds to one cell. **D** Live cell imaging spinning disk confocal microscopy of PI4P (mCherry-P4MSiDM) during cytokinesis in WT HeLa cells (top), or cells expressing GFP-ORP3-ΔORD (green, bottom).

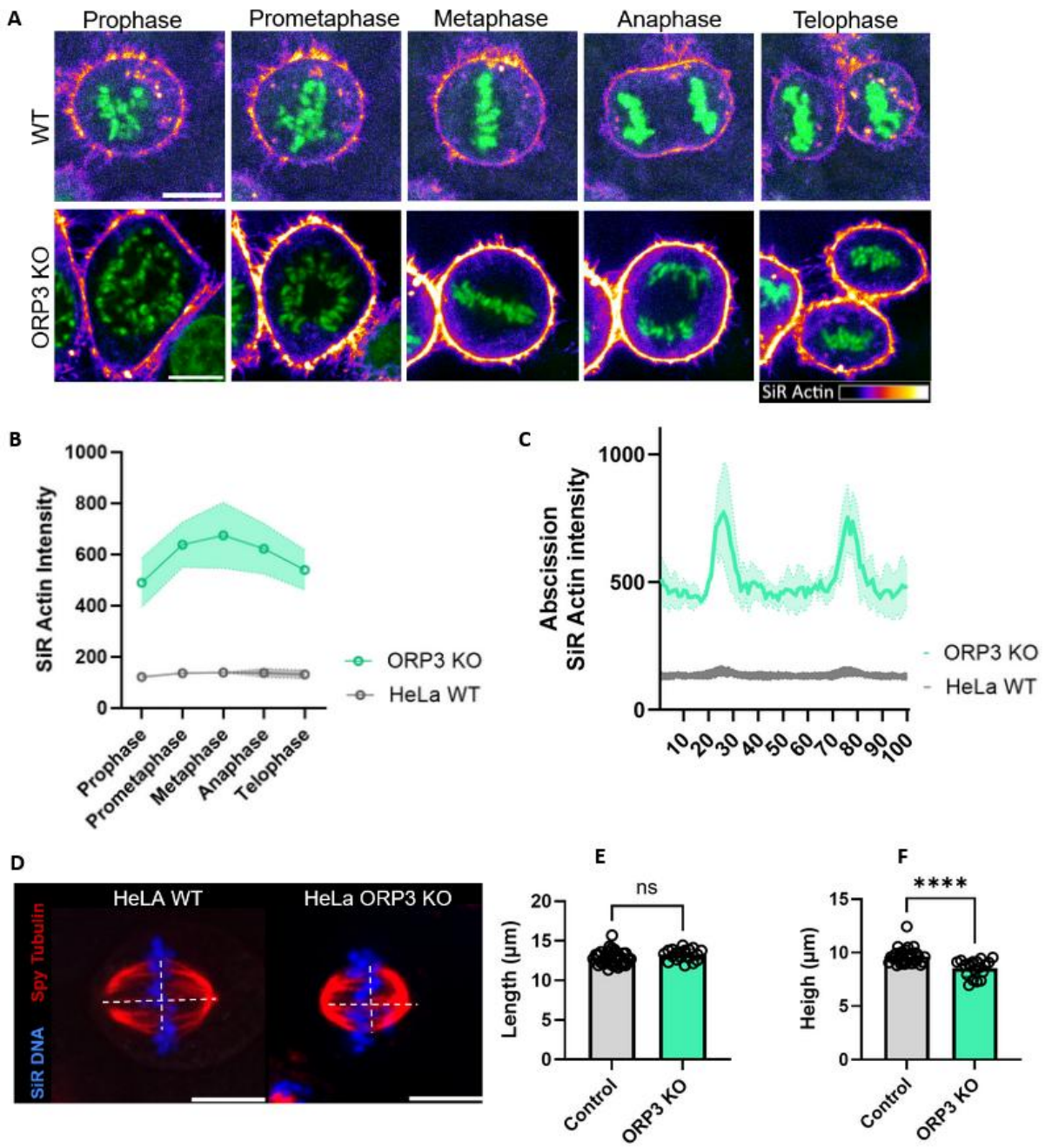

Figure 6 – ORP3 is required for actin and tubulin distribution in mitosis.

A Live cell imaging spinning disk confocal microscopy of actin (Sir Actin) and DNA (Spy-DNA). Bar = 20µm. **B** - Quantification of the average actin signal at the cortex across mitotic phases. Shades: SEM **C** Quantification of the actin signal intensity along the cortex in cytokinesis. Membrane length was normalized with position 0/100 corresponding to each pole and 25 (and 75) to one on the two side of the equatorial plane. Shades: SEM **D** Fluorescence staining of mitotic furrow in WT and ORP3 KO cells. **E** Length of the mitotic furrow in control

and ORP3 KO cell lines (n=3). **F** Width of the mitotic furrow in control and ORP3 KO cell lines (n=3).

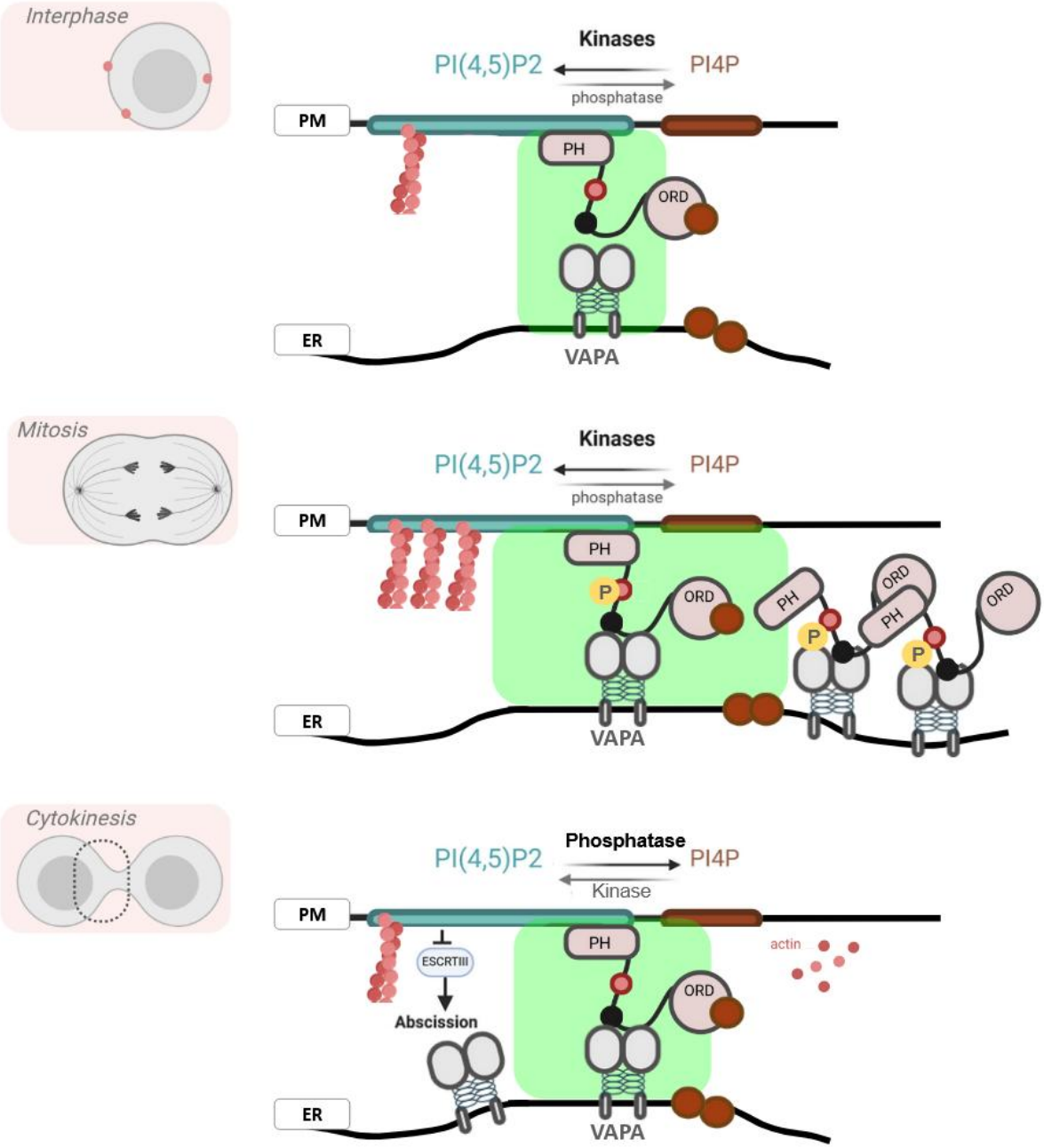
Interphase
Kinases
PI(4,5)P2
PI4P
phosphatase
PM
PH
ORD
ER
VAPA
Mitosis
Kinases
PI(4,5)P2
PI4P
phosphatase
PM
PH
P
ORD
PH
ORD
PH
ORD
P
P
ER
VAPA
Cytokinesis
Phosphatase
PI(4,5)P2
PI4P
Kinase
PM
ESCRTIII
Abscission
PH
ORD
actin
ER
VAPA

Figure 7– Proposed function and regulation of ORP3 regulation in the cell cycle.

In interphase (top panel), ORP3 is only weakly associated to the ER and only to PI(4,5)P2 rich plasma membrane domains. ORP3 interaction domains as well as the inter-conversion between PI4P and PI(4,5)P2 by phosphatases and kinases can be regulated by intracellular signaling. During mitosis (middle panel), the FFAT-like domain is phosphorylated and ER-association of ORP3 is strongly enhanced. Since plasma membrane PI(4,5)P2 levels are also increased the plasma membrane, association of ORP3 at ER-plasma membrane contacts is potentiated. Following ORP3 “priming” at contact sites, the regulation of PI4P and PI(4,5)P2 becomes highly dependent on local phosphatases and kinases. At the end of cytokinesis, ORP3 is associated to the cytoplasmic bridge. Phosphatases such as OCRL are activated in order to hydrolyze PI(4,5)P2 into PI4P and ORP3 function allows to drain and deplete PI4P from the plasma membrane at the cytoplasmic bridge.

REFERENCES

Antonny, Bruno, Joelle Bigay, et Bruno Mesmin. 2018. « The Oxysterol-Binding Protein Cycle: Burning Off PI(4)P to Transport Cholesterol. » Annual Review of Biochemistry 87 (juin): 809-37. https://doi.org/10.1146/annurev-biochem-061516-044924.

Bugda Gwilt, Katlynn, et Jay R. Thiagarajah. 2022. « Membrane Lipids in Epithelial Polarity: Sorting out the PIPs ». Frontiers in Cell and Developmental Biology 10: 893960. https://doi.org/10.3389/fcell.2022.893960.

Carim, Sabrya C., Khaled Ben El Kadhi, Guanhua Yan, et al., 2019. « IPIP27 Coordinates PtdIns(4,5)P2 Homeostasis for Successful Cytokinesis ». Current Biology 29 (5): 775-789.e7. https://doi.org/10.1016/j.cub.2019.01.043.

Cauvin, Clothilde, et Arnaud Echard. 2015. « Phosphoinositides: Lipids with Informative Heads and Mastermind Functions in Cell Division. » Biochimica et Biophysica Acta 1851 (6): 832-43. https://doi.org/10.1016/j.bbalip.2014.10.013.

Chang, Chi-Lun, Ting-Sung Hsieh, T. Tony Yang, et al., 2013. « Feedback Regulation of Receptor-Induced Ca2+ Signaling Mediated by E-Syt1 and Nir2 at Endoplasmic Reticulum-Plasma Membrane Junctions ». Cell Reports 5 (3): 813-25. https://doi.org/10.1016/j.celrep.2013.09.038.

Chen, J., and J. Liu. 2016. Spindle Size Scaling Contributes to Robust Silencing of Mitotic Spindle Assembly Checkpoint. *Biophysical Journal*. 111:1064–1077. doi:10.1016/j.bpj.2016.07.039.

Chung, Jeeyun, Federico Torta, Kaori Masai, et al., 2015. « INTRACELLULAR TRANSPORT. PI4P/Phosphatidylserine Countertransport at ORP5- and ORP8-Mediated ER-Plasma Membrane Contacts ». Science (New York, N.Y.) 349 (6246): 6246. https://doi.org/10.1126/science.aab1370.

Dambournet, Daphné, Mickael Machicoane, Laurent Chesneau, et al., 2011. « Rab35 GTPase and OCRL Phosphatase Remodel Lipids and F-Actin for Successful Cytokinesis ». Nature Cell Biology 13 (8): 981-88. https://doi.org/10.1038/ncb2279.

D'Souza, Ryan S., Jun Y. Lim, Alper Turgut, et al., 2020. « Calcium-Stimulated Disassembly of Focal Adhesions Mediated by an ORP3/IQSec1 Complex ». eLife 9 (avril): e54113. https://doi.org/10.7554/eLife.54113.

Delfosse, V, Bourguet, W, and Drin, G (2020). Structural and Functional Specialization of OSBP-Related Proteins - Vanessa Delfosse, William Bourguet, Guillaume Drin, 2020. Available at: https://journals.sagepub.com/doi/full/10.1177/2515256420946627. Accessed July 7, 2025.

Di Mattia, T, Wilhelm, LP, Ikhlef, S, Wendling, C, Spehner, D, Nominé, Y, Giordano, F, Mathelin, C, Drin, G, Tomasetto, C, *et al.*, (2018). Identification of MOSPD2, a novel scaffold for endoplasmic reticulum membrane contact sites. EMBO Reports 19, e45453.

Fehon, RG, McClatchey, AI, and Bretscher, A (2010). Organizing the cell cortex: the role of ERM proteins. Nat Rev Mol Cell Biol 11, 276–287.

Gassama-Diagne, Ama, Wei Yu, Martin ter Beest, et al., 2006. « Phosphatidylinositol-3,4,5-Trisphosphate Regulates the Formation of the Basolateral Plasma Membrane in Epithelial Cells ». Nature Cell Biology 8 (9): 963-70. https://doi.org/10.1038/ncb1461.

Gervais, Louis, Sandra Claret, Jens Januschke, Siegfried Roth, et Antoine Guichet. 2008. « PIP5K-dependent production of PIP2 sustains microtubule organization to establish polarized transport in the Drosophila oocyte ». Development 135 (23): 3829-38. https://doi.org/10.1242/dev.029009.

Gulyás, Gergő, Mira Sohn, Yeun Ju Kim, Péter Várnai, et Tamas Balla. 2020. « ORP3 phosphorylation regulates phosphatidylinositol 4-phosphate and Ca2+ dynamics at plasma membrane–ER contact sites ». Journal of Cell Science 133 (6): jcs237388. https://doi.org/10.1242/jcs.237388.

Hara, Y., and A. Kimura. 2013. An allometric relationship between mitotic spindle width, spindle length, and ploidy in Caenorhabditis elegans embryos. *Mol Biol Cell*. 24:1411–1419. doi:10.1091/mbc.E12-07-0528.

Jackson, Catherine L., Laurence Walch, et Jean-Marc Verbavatz. 2016. « Lipids and Their Trafficking: An Integral Part of Cellular Organization. » Developmental Cell 39 (2): 139-53. https://doi.org/10.1016/j.devcel.2016.09.030.

Kim, SoHui, Amir Kedan, Merav Marom, et al., 2013. « The phosphatidylinositol-transfer protein Nir2 binds phosphatidic acid and positively regulates phosphoinositide signalling ». EMBO Reports 14 (10): 891-99. https://doi.org/10.1038/embor.2013.113.

Kim, Yeun Ju, Maria-Luisa Guzman-Hernandez, Eva Wisniewski, et Tamas Balla. 2015. « Phosphatidylinositol-Phosphatidic Acid Exchange by Nir2 at ER-plasma membrane Contact Sites Maintains Phosphoinositide Signaling Competence ». Developmental Cell 33 (5): 549-61. https://doi.org/10.1016/j.devcel.2015.04.028.

Kletter, T., S. Reusch, T. Cavazza, N. Dempewolf, C. Tischer, and S. Reber. 2022. Volumetric morphometry reveals spindle width as the best predictor of mammalian spindle scaling. *J Cell Biol*. 221:e202106170. doi:10.1083/jcb.202106170.

Kotak, Sachin, Coralie Busso, et Pierre Gönczy. 2014. « NuMA Interacts with Phosphoinositides and Links the Mitotic Spindle with the Plasma Membrane ». The EMBO Journal 33 (16): 1815-30. https://doi.org/10.15252/embj.201488147.

Kunda, P., A.E. Pelling, T. Liu, and B. Baum. 2008. Moesin controls cortical rigidity, cell rounding, and spindle morphogenesis during mitosis. *Curr Biol*. 18:91–101. doi:10.1016/j.cub.2007.12.051.

Lachat, J., A. Pascault, D. Thibaut, R. Le Borgne, J.-M. Verbavatz, and A. Weiner. 2022. Trans-cellular tunnels induced by the fungal pathogen Candida albicans facilitate invasion through successive epithelial cells without host damage. *Nat Commun*. 13:3781. doi:10.1038/s41467-022-31237-z.

Lehto, M., M.I. Mayranpaa, T. Pellinen, P. Ihalmo, S. Lehtonen, P.T. Kovanen, P.-H. Groop, J. Ivaska, and V.M. Olkkonen. 2008. The R-Ras interaction partner ORP3 regulates cell adhesion. *J Cell Sci*. 121:695–705. doi:10.1242/jcs.016964.

Lehto, Markku, Riikka Hynynen, Katja Karjalainen, Esa Kuismanen, Kati Hyvärinen, et Vesa M. Olkkonen. 2005. « Targeting of OSBP-related protein 3 (ORP3) to endoplasmic reticulum and plasma membrane is controlled by multiple determinants ». Experimental Cell Research 310 (2): 445-62. https://doi.org/10.1016/j.yexcr.2005.08.003.

Logan, Michael R., et Craig A. Mandato. 2006. « Regulation of the Actin Cytoskeleton by PIP2 in Cytokinesis ». Biology of the Cell 98 (6): 377-88. https://doi.org/10.1042/BC20050081.

Machicoane, M, de Frutos, CA, Fink, J, Rocancourt, M, Lombardi, Y, Garel, S, Piel, M, and Echard, A (2014). SLK-dependent activation of ERMs controls LGN-NuMA localization and spindle orientation. J Cell Biol 205, 791–799.

Mandal, Kalpana. 2020. « Review of PIP2 in Cellular Signaling, Functions and Diseases ». International Journal of Molecular Sciences 21 (21): 8342. https://doi.org/10.3390/ijms21218342.

Mesmin, Bruno, Joelle Bigay, Joachim Moser von Filseck, Sandra Lacas-Gervais, Guillaume Drin, et Bruno Antonny. 2013. « A Four-Step Cycle Driven by PI(4)P Hydrolysis Directs Sterol/PI(4)P Exchange by the ER-Golgi Tether OSBP. » Cell 155 (4): 830-43. https://doi.org/10.1016/j.cell.2013.09.056.

Mesmin, Bruno, Joelle Bigay, Joel Polidori, Denisa Jamecna, Sandra Lacas-Gervais, et Bruno Antonny. 2017. « Sterol Transfer, PI4P Consumption, and Control of Membrane Lipid Order by Endogenous OSBP. » The EMBO Journal 36 (21): 3156-74. https://doi.org/10.15252/embj.201796687.

Moser von Filseck, Joachim, Bruno Mesmin, Joelle Bigay, Bruno Antonny, et Guillaume Drin. 2014. « Building Lipid “PIPelines” throughout the Cell by ORP/Osh Proteins. » Biochemical Society Transactions 42 (5): 1465-70. https://doi.org/10.1042/BST20140143.

Njeru, Sospeter N., Johann Kraus, Jitendra K. Meena, et al., 2020. « Aneuploidy-Inducing Gene Knockdowns Overlap with Cancer Mutations and Identify Orp3 as a B-Cell Lymphoma Suppressor ». Oncogene 39 (7): 1445-65. https://doi.org/10.1038/s41388-019-1073-2.

Olkkonen, Vesa M. 2015. « OSBP-Related Protein Family in Lipid Transport Over Membrane Contact Sites ». Lipid insights 8 (Suppl 1): 1-9. https://doi.org/10.4137/LPI.S31726.

Posor, York, Wonyul Jang, et Volker Haucke. 2022. « Phosphoinositides as Membrane Organizers ». Nature Reviews Molecular Cell Biology 23 (12): 797-816. https://doi.org/10.1038/s41580-022-00490-x.

Puhka, Maija, Helena Vihinen, Merja Joensuu, et Eija Jokitalo. 2007. « Endoplasmic reticulum remains continuous and undergoes sheet-to-tubule transformation during cell division in mammalian cells ». Journal of Cell Biology 179 (5): 895-909. https://doi.org/10.1083/jcb.200705112.

Reinisch, Karin M., et William A. Prinz. 2021. « Mechanisms of Nonvesicular Lipid Transport ». The Journal of Cell Biology 220 (3): e202012058. https://doi.org/10.1083/jcb.202012058.

Roubinet, C, Decelle, B, Chicanne, G, Dorn, JF, Payrastre, B, Payre, F, and Carreno, S (2011). Molecular networks linked by Moesin drive remodeling of the cell cortex during mitosis. Journal of Cell Biology 195, 99–112.

Senju, Yosuke, et Pekka Lappalainen. 2019. « Regulation of actin dynamics by PI(4,5)P2 in cell migration and endocytosis ». Current Opinion in Cell Biology, Cell Architecture, vol. 56 (février): 7-13. https://doi.org/10.1016/j.ceb.2018.08.003.

Siegfried, Hugo, Georges Farkouh, Rémi Le Borgne, et al., 2024. « The ER Tether VAPA Is Required for Proper Cell Motility and Anchors ER-plasma membrane Contact Sites to Focal Adhesions ». eLife 13 (mars): e85962. https://doi.org/10.7554/eLife.85962.

Sohn, M., M. Korzeniowski, J.P. Zewe, R.C. Wills, G.R.V. Hammond, J. Humpolickova, L. Vrzal, D. Chalupska, V. Veverka, G.D. Fairn, E. Boura, and T. Balla. 2018. PI(4,5)P2 controls plasma membrane PI4P and PS levels via ORP5/8 recruitment to ER–PM contact sites. *J Cell Biol*. 217:1797–1813. doi:10.1083/jcb.201710095.

Solinet, S., K. Mahmud, S.F. Stewman, K. Ben El Kadhi, B. Decelle, L. Talje, A. Ma, B.H. Kwok, and S. Carreno. 2013. The actin-binding ERM protein Moesin binds to and stabilizes microtubules at the cell cortex. *J Cell Biol*. 202:251–260. doi:10.1083/jcb.201304052.

Tong, Junsen, Lingchen Tan, et Young Jun Im. 2021. « Structure of Human ORP3 ORD Reveals Conservation of a Key Function and Ligand Specificity in OSBP-Related Proteins ». PloS One 16 (4): e0248781. https://doi.org/10.1371/journal.pone.0248781.

Wang, Xue, Junnan Liu, Anca Azoitei, et al., 2023. « Loss of ORP3 Induces Aneuploidy and Promotes Bladder Cancer Cell Invasion through Deregulated Microtubule and Actin Dynamics ». Cellular and Molecular Life Sciences 80 (10): 299. https://doi.org/10.1007/s00018-023-04959-6.

Weber-Boyvat, Marion, Henriikka Kentala, Johanna Lilja, et al., 2015. « OSBP-Related Protein 3 (ORP3) Coupling with VAMP-Associated Protein A Regulates R-Ras Activity ». Experimental Cell Research 331 (2): 278-91. https://doi.org/10.1016/j.yexcr.2014.10.019.

Xu, Pengfei, Julia Richter, Annette Blatz, et al., 2020. « Downregulation of ORP3 Correlates with Reduced Survival of Colon Cancer Patients with Advanced Nodal Metastasis and of Female Patients with Grade 3 Colon Cancer ». International Journal of Molecular Sciences 21 (16): E5894. https://doi.org/10.3390/ijms21165894.

Yang, Y., M. Lee, and G.D. Fairn. 2018. Phospholipid subcellular localization and dynamics. *Journal of Biological Chemistry*. 293:6230–6240. doi:10.1074/jbc.R117.000582.

Yu, F., and K. Machaca. 2025. Remodeling of ER Membrane Contact Sites During Cell Division. *Contact (Thousand Oaks)*. 8:25152564241309207. doi:10.1177/25152564241309207.

Zieve, G W, S R Heidemann, et J R McIntosh. 1980. « Isolation and Partial Characterization of a Cage of Filaments That Surrounds the Mammalian Mitotic Spindle. » The Journal of Cell Biology 87 (1): 160-69. https://doi.org/10.1083/jcb.87.1.160.